Title: Adolescent parvalbumin expression in the left orbitofrontal cortex shapes sociability in female mice

Abbreviated title: OFC_L parvalbumin expression and female sociability

Authors: Yi-Seon Jeon[1†], Daun Jeong[1†], Hanseul Kweon[1,2], Jae-Hyun Kim[1], Choong Yeon Kim[3], Youngbin Oh[1], Young-Ho Lee[1], Chan Hyuk Kim[1], Sang-Gyu Kim[1], Jae-Woong Jeong[3], Eunjoon Kim[1,2], and Seung-Hee Lee[1,2*]

Affiliations:

[1]Department of Biological Sciences, KAIST, 291 Daehak-ro, Yuseong-gu, Daejeon, 34141, Korea

[2]Center for Synaptic Brain Dysfunctions, Institute for Basic Science, KAIST, 291 Daehak-ro, Yuseong-gu, Daejeon, 34141, Korea

[3]School of Electrical Engineering, KAIST, 291 Daehak-ro, Yuseong-gu, Daejeon, 34141, Korea

[†]These authors contributed equally to this work.

*Correspondence: shlee1@kaist.ac.kr (S.-H. L.)

The number of pages: 55

The number of figures: 7

The number of words for abstract: 247 words

The number of words for introduction: 623 words

The number of words for discussion: 1463 words

Conflict of interest

The authors declare no competing financial interests.

Acknowledgments

This work was supported by grants from the National Research Foundation of Korea (2021R1A2C3012159, 2021R1A4A2001803, to S.-H.L. and 2021R1A2C4001483, to J.-W.J.) and the KAIST Global Singularity Program for 2020 (to S.-H.L.). This work was also supported by the Rural Development Administration (PJ016403, to S.K.) and by the Institute for Basic Science (IBS-002-D1 to E.K. and IBS-002-D3 to S.-H.L.). We thank all members of the Lee laboratory for their helpful discussion, Dr. Soo Young Kim for discussion on the PWSI, and Emily Wheeler, Boston, for editorial assistance.

Abstract

The adolescent social experience is essential for the maturation of the prefrontal cortex in mammalian species. However, it still needs to be determined which cortical circuits mature with such experience and how it shapes adult social behaviors in a sex-specific manner. Here, we examined social approaching behaviors in male and female mice after post-weaning social isolation (PWSI), which deprives social experience during adolescence. We found that the PWSI, particularly isolation during late adolescence, caused an abnormal increase in social approaches (hypersociability) only in female mice. We further found that the PWSI female mice showed reduced parvalbumin (PV) expression in the left orbitofrontal cortex (OFC_L). When we measured neural activity in the female OFC_L, a substantial number of neurons showed higher activity when mice sniffed other mice (social sniffing) than when they sniffed an object (object sniffing). Interestingly, the PWSI significantly reduced both the number of activated neurons and the activity level during social sniffing in female mice. Similarly, the CRISPR/Cas9-mediated knock-down of PV in the OFC_L during late adolescence enhanced sociability and reduced the social sniffing-induced activity in adult female mice via decreased excitability of PV^+ neurons and reduced synaptic inhibition in the OFC_L. Moreover, optogenetic activation of excitatory neurons or optogenetic inhibition of PV^+ neurons in the OFC_L enhanced sociability in female mice. Our data demonstrate that the adolescent social experience is critical for the maturation of PV^+ inhibitory circuits in the OFC_L; this maturation shapes female social behavior via enhancing social representation in the OFC_L.

53 **Significance Statement**

54 Adolescent social isolation often changes adult social behaviors in mammals. Yet, we do not fully
55 understand the sex-specific effects of social isolation and the brain areas and circuits that mediate
56 such changes. Here, we found that adolescent social isolation causes three abnormal phenotypes
57 in female but not male mice: hypersociability, decreased PV^+ neurons in the OFC_L, and decreased
58 socially evoked activity in the OFC_L. Moreover, PV deletion in the OFC_L *in vivo* caused the same
59 phenotypes in female mice by increasing excitation compared with inhibition within the OFC_L.
60 Our data suggest that adolescent social experience is required for PV maturation in the OFC_L,
61 which is critical for evoking OFC_L activity that shapes social behaviors in female mice.

62 **Introduction**

63 One of the hallmarks of postnatal maturation in the mammalian cortex is the maturation of
64 GABAergic inhibitory circuits (Luhmann and Prince, 1991). Maturation is accompanied by an
65 increase in the expression of both the parvalbumin (PV) in a subset of GABAergic neurons and
66 the perineuronal nets (PNNs) surrounding the PV^+ neurons (Celio and Blumcke, 1994; Huang et
67 al., 1999). PV is a calcium-binding protein and a well-known genetic marker for fast-spiking
68 GABAergic neurons in the cortex (Rudy et al., 2011). PV gene expression is upregulated in the
69 sensory cortex in an activity-dependent manner (Sugiyama et al., 2008; Krishnan et al., 2017) after
70 mammals are born. Like PV, PNNs also increase during cortical maturation and, in the adult cortex,
71 surround most of the PV^+ neurons (Ueno et al., 2017; Ueno et al., 2018). Along with the increase
72 of PNNs in cortical circuits, other molecular changes reduce net plasticity and facilitate the
73 maturation of the cortical network (Beurdeley et al., 2012). If mice are deprived of visual input
74 during the critical period after eye opening, via monocular deprivation or dark rearing, PV^+
75 neurons are less developed, and PNNs are reduced in the primary visual cortex (V1) (Sugiyama et
76 al., 2008). This deprivation, in turn, diminishes both the visual response of V1 neurons that receive
77 input from the deprived eye (Sugiyama et al., 2008) and inhibition in the cortex (Dityatev et al.,
78 2007). Therefore, the postnatal sensory experience is critical for the expression of PV and PNNs
79 in PV^+ neurons, as these are required for the maturation of PV^+ inhibitory circuits and, eventually,
80 for shaping sensory responses in the cortex (Hensch, 2005).

81 The maturation of the cortex occurs first in the sensory area, where the process is part of
82 sensory experience, and later in the motor-frontal and the PFC (Hensch, 2005). The social
83 experience is critical for the maturation of the PFC in both humans (Blakemore, 2008; Paus et al.,
84 2008) and rodents (Makinodan et al., 2012; Bicks et al., 2020; Tan et al., 2021), particularly during

85 juvenile and adolescent periods. Patients with autism or schizophrenia often show abnormal social
86 cognition as well as dysfunction in the PFC (Bicks et al., 2015). In these patients, the expression
87 of PV and PNNs is reduced in the dorsolateral PFC (Enwright et al., 2016). Thus, it is plausible
88 that immature PV^+ circuits in the PFC cause the psychiatric symptoms underlying abnormal social
89 behavior in mammals. However, we still do not understand whether social experience is required
90 for PV^+ inhibitory circuits in these PFC regions to mature. In particular, it is largely unknown
91 whether social experience affects the maturation of inhibitory circuits in the orbitofrontal cortex
92 (OFC), one of the PFC sub-regions critical for social cognition (Adolphs, 2003; Amodio and Frith,
93 2006).

94 Mammalian social behavior is important for maintaining a conspecific society. Social
95 interaction during adolescence is critical for shaping social and cognitive behaviors in both humans
96 and rodents (Spear, 2000; Makinodan et al., 2012; Hinton et al., 2019; Almeida et al., 2021;
97 Potrebic et al., 2022). Interestingly, the mammalian brain shows hemispheric asymmetry and
98 lateralization in executing social behaviors (Marlin et al., 2015). Even in rodents, according to
99 recent studies, the PFC functions asymmetrically in mediating social behaviors (Lee et al., 2015;
100 Marlin et al., 2015). However, whether such asymmetry in the PFC becomes increasingly
101 pronounced in a sex-specific manner with social experience during adolescence is still unclear.
102 We investigated the effect of adolescent social isolation on the maturation of PV^+ neurons in the
103 PFC in both sexes and hemispheres. Using post-weaning social isolation (PWSI) and the
104 CRISPR/Cas9 system, we revealed that social isolation during adolescence caused the defect in
105 PV expression in the OFC_L of female mice, which led to hypersociability and reduced OFC_L
106 activity during social contact.

Materials and Methods

Experimental model and subject details

We approved all experimental procedures from the KAIST Institutional Animal Care and Use Committee (IACUC-18-236). We maintained all mice ad libitum under light from 8 am to 8 pm and dark cycle from 8 pm to 8 am. All mice were weaned at postnatal day 21 (P21); mice were reared in double (28cm × 17cm × 14cm) cages with 3-5 mates for group housing or in single (20cm × 10cm × 14cm) cages alone for social isolation. We performed experiments on WT (C57BL/6J), PV-Cre (JAX, #008069), and the Rosa26-floxed STOP-Cas9 knock-in (JAX # 024857) mice.

Histology

We anesthetized mice with isoflurane and then perfused them with 1X phosphate-buffered saline (PBS) and 4% paraformaldehyde (PFA, w/v in PBS). Mouse brain samples were post-fixed for 4h at 4℃; after fixation, we incubated them in 30% sucrose solution (w/v in PBS) for 1-2 days at 4℃. Then, we embedded each brain sample in an optimal cutting temperature medium (OCT, Tissue-Tek, Cat#4583) and froze each at -80℃. We sectioned frozen brains using a cryostat (Leica) and collected coronal sections either at 30 μm (for confirming injection sites) or 15 μm (for immunostaining) thickness. To confirm fluorescently labeled injection sites, brain sections were washed three times with 1X PBS and mounted in DAPI-containing mounting medium (VECTASHIELD®, cat#H-1200). For immunostaining, we washed the brain sections three times with 1X PBS and permeabilized them with 0.3% Triton X-100 in 1X PBS for 30 min. After the sections were incubated in a blocking solution (2% normal donkey serum in 1X PBS) for 2 hours

128 at room temperature, we incubated them with primary antibodies (rabbit anti-PV, 1:500 dilution
129 in blocking solution, Swant, cat#PV25; mouse anti-NeuN, 1:500 dilution in blocking solution,
130 Millipore, cat#MAB377) for 2 days at 4℃. Last, we incubated them with fluorescence-tagged
131 secondary antibodies (Alexa Fluor 594 donkey anti-rabbit IgG for PV staining, 1:500 dilution in
132 1X PBS, Life Technology, cat#A21207; Alexa Fluor 647 donkey anti-mouse IgG for NeuN
133 staining, 1:500 dilution in 1X PBS, Jackson Immunoresearch, cat#715-605-151). For PNN
134 staining, we treated the brain sections with the Fluorescein (FITC) labeled Wisteria Floribunda
135 Lectin (WFA, WFL) (1:500 dilution in 1X PBS, Vector labs, cat#FL-1351) for 2 hours at RT
136 before mounting them in clear mounting medium (DAKO, cat#S3023). We imaged fluorescent
137 signals of mounted brain sections under a scanning microscope (ZEISS, Axio Scan.Z1).

138 **Cell counting analysis**

139 When we sectioned the mouse brain samples, we collected 15μm brain sections in every
140 60μm thickness across the frontal cortex. After immunostaining the sections, we scanned the
141 fluorescent images of the brain sections and matched the images to the mouse brain atlas (Franklin
142 and Paxinos) to confirm the anterior-to-posterior location of the coronal brain sections. We then
143 selected three images of sections in a row that include OFC areas (between +2.10mm ~ +2.34mm
144 anterior from the bregma) (see Fig 2C). To count the labeled neurons in the OFC, we put a 0.3 x
145 $0.3mm^2$ square as a region of interest (ROI) at the center of the OFC (±1.3mm lateral from the
146 bregma; depth, -2.5mm). To quantify the number of PV^+ and $NeuN^+$ neurons, we used the
147 automatic cell counting software (ImageJ) (Grishagin, 2015). After converting the fluorescent
148 images to the 8-bit grayscale images, we further transformed the grayscale images into binary
149 images. For the binary transition, we used distinct thresholds at the grayscale for isolating the

150 NeuN$^+$ neurons (Fig. 2, 11.39±0.02% of total mean intensity) and the PV$^+$ neurons (Fig. 2,
151 2.12±0.16% of total mean intensity). We then automatically counted the white-filled circles as
152 cells if they satisfied the following conditions: 1) the total size is above 60 x 60 pixels, and 2) the
153 circularity is above 0.2. We set the thresholds in each sample at the level that yielded a similar
154 number of cells from the automatic counting compared to the manual counting using a couple of
155 template images from each sample. There was no significant difference between the number of
156 cells counted automatically and the number of cells counted manually in a blind manner (see Fig.
157 2B). To validate the knock-down efficiency of sgPV or chABC (see Fig 5), we manually and
158 blindly counted the number of PV$^+$ or WFA$^+$ neurons in the ROI.

159 **Sociability test**

160 We performed the sociability test by using two types of mazes: one is a modified 3-
161 chamber-like maze (50cm × 45cm × 20cm) where two containers were located diagonally at
162 opposite corners, and the other is a standard 3-chamber maze (60cm x 40cm x 20cm), which was
163 used in other literature (Won et al., 2012). Most of the data we plotted in the manuscript were
164 collected in the modified maze. We performed the sociability test on mice at either P79-81 or P50.
165 Before behavior experiments, all mice were habituated for 30-60 minutes in the habituation
166 chamber. All mice were maintained in a group-housed or an isolated condition until the habituation.
167 Mice were then moved to the sociability test maze. The sociability test consisted of two phases: 1)
168 habituation in the sociability maze (empty containers, 10min) and 2) sociability test (an object
169 container and a social container with a stranger mouse, 10min). We used a 2-week younger and
170 same-sex mouse as a stranger mouse not to evoke any aggressively or sexually driven social
171 behaviors in the tested mouse (Murugan et al., 2017). We used the software, EthoVision®XT 11.5
172 (Noldus), to automatically analyze interaction times and manually analyze the sniffing time. The

173 sniffing time was defined as the time when the subject mouse's nose contacted the container either
174 empty or with a novel mouse. We analyzed mouse sociability by two indicators: time spent in
175 interaction zones near the container (18cm × 18cm) and sniffing time. We calculated the social
176 sniffing and social interaction indices as follows (Nakanishi et al., 2017; Cheong et al., 2020):

177 $$\text{Social sniffing index} = \frac{(Social\ sniffing\ time)}{(Object\ sniffing\ time) + (Social\ sniffing\ time)}$$

178 $$\text{Social interaction index} = \frac{(Time\ in\ social\ zone)}{(Time\ in\ object\ zone) + (Time\ in\ social\ zone)}$$

179 **Resident-intruder (RI) test**

180 We devised the resident-intruder (RI) test as previously described (Tan et al., 2021). The
181 mouse was single-housed for 24hr and then exposed to an intruder mouse in the home cage for 10
182 minutes. We used a slightly smaller (10-20% lighter) unfamiliar sex- and strain-matched novel
183 mouse as an intruder. The offensive behaviors of the subject mouse against the intruder, including
184 lateral threat, upright posture, clinch attack, and chase, were scored as aggressive behaviors. In
185 addition, the non-offensive social behaviors in the RI test, such as nose-to-nose interaction and
186 anogenital sniffing, were scored. All scoring was performed blindly.

187 **Measuring estrous cycle in female mice**

188 We monitored the estrous cycle of female mice using vaginal cytology (McLean et al.,
189 2012). Vaginal smears from subject mice were collected right after the sociability test. Smears
190 were placed on slides and stained with 0.1% crystal violet (Sigma Aldrich, cat#V5265). Each
191 estrous cycle stage was determined based on the cell type that was mainly observed in the smear
192 sample among the three types: nucleated epithelial cells, cornified squamous epithelial cells, and

193 leukocytes. To examine the difference in estrous cycles between GH and PWSI, we performed the
194 vaginal cytology for four consecutive days in each mouse.

195 ***In vivo* extracellular recordings for measuring sniffing-induced activity**

196 We performed all recordings in the head-fixed and awake mice. We marked the top of left
197 and right OFCs and implanted custom-designed head-plates on the skull of mice using dental
198 cement and small screws. After 2-3 days of recovery, we habituated mice to be head-fixed for
199 20min per day for 3 days. After the habituation, we performed the recording in the OFC by making
200 a small craniotomy on the marked spots and inserting 32 channel silicon probes (A1X32-Poly2-
201 10mm-50-177 or A1X32-Poly3-10mm-50-177, Neuronexus) vertically into each OFC using a
202 micro-drive manipulator (Siskiyou). We first recorded spiking activity in the OFC without
203 presenting a stranger mouse for 10 min ($object_{sniffing}$ session) and next continuously recorded
204 neural activity while presenting a head-fixed stranger mouse in front of the recorded mouse for 10
205 min ($social_{sniffing}$ session). During the recording, we monitored and recorded the sniffing behavior
206 of the mouse by using a web camera (Microsoft, LifeCam HD-3000). All extracellular signals were
207 recorded at a 30kHz sampling rate, filtered between 500~5000Hz, and amplified by a miniature
208 digital headstage (CerePlex μ, Blackrock Microsystems). After the recording, we confirmed the
209 recording sites by injecting red retrobeads (Lumaflour) into the recording areas and performing
210 histology. If the recording sites were outside of the OFC, we did not use those recording data in
211 further analysis.

212 *Automatic quantification of sniffing behaviors*

213 We developed a Matlab code to automatically analyze sniffing events during object- and
214 social sniffing sessions in head-fixed mice. First, we converted all the RGB image frames of a

recorded video clip to grayscale using the '*rgb2gray*' function. Next, we chose the region of interest (ROI), including the nose and whiskers of the mouse being recorded, made a binary matrix with 1 inside the ROI and 0 outside the ROI of each pixel, and multiplied an original image by the binary matrix of each corresponding pixel along all the frames (ROI_1). We subtracted background brightness from ROI_1 to eliminate overall brightness fluctuations (ROI_2) and calculated deviations of brightness within the ROI by subtracting the mean brightness of each pixel (ROI ΔF). To detect sniffing events, we subtracted a moving average (F_0, sliding window = 50 frames) from ROI ΔF (ROI $\Delta F–F_0$), and set a threshold by multiplying a median of absolute ROI $\Delta F–F_0$ by 4. If ROI $\Delta F–F_0$ in each frame crossed the threshold, we included the frame in a sniffing event.

Neural activity analysis

We performed the spike-sorting using Klusters software (http://neurosuite.sourceforge.net/) (Hazan et al., 2006). We grouped 32-channel data into eight groups and sorted single units by principal components analysis. We only isolated single units that show more than a 2 ms refractory period in their auto-correlogram. We performed all other analyses using custom-made codes in Matlab (Mathworks). We sorted sniffing trials in object and social sessions by identifying sniffing events across the recording sessions. We only used trials that satisfied the following two criteria: 1) inter-sniffing interval (time between the offset of sniffing in the current trial and the onset time of the next trial) > 5sec, and 2) sniffing duration (time between the onset and the offset of sniffing in one trial) > 1sec. To plot the peri-event time histogram (PETH) of all neurons as a population, we performed Z-scoring by averaging firing rates (Hz) of individual units across trials and normalized them by 1sec baseline activity (3 to 2 sec before the onset of sniffing). The normalized firing rates were convolved with a Gaussian filter (σ = 50ms) only for visualization purposes. To

238 identify the neurons showing significant sniffing-induced activity, we statistically compared the
239 firing rates of individual neurons during the 2-sec pre-period (3 to 1 sec before the onset of sniffing)
240 and 2-sec post-period (0 to 2 sec after the onset of sniffing) of each sniffing trial by bootstrapping
241 ($p < 0.01$, $n = 5000$). We quantified the sniffing-induced activity of neurons by averaging Z values
242 from 0 to 2 sec after the onset of sniffing. We classified cell types of recorded neurons based on
243 spike waveforms by quantifying spike widths of each isolated neuron (time between peak and
244 through of the spike, μs). If the spike width was below 350 μs or above 450 μs, recorded neurons
245 were classified as fast-spiking (FS) neurons or regular-spiking (RS) neurons, respectively. For the
246 baseline activity analysis, we quantified the average firing rates (Hz) from 0 to 2 sec before the
247 onset of sniffing.

248 **Perineuronal net degradation**

249 To remove the PNN, we reconstituted protease-free chABC (Amsbio) in PBS to a final
250 concentration of 61U/ml. We anesthetized mice by inhalation of 1.5 % isoflurane in oxygen on the
251 stereotaxic apparatus. We injected 0.5μl of PBS or chABC into the left OFC (AP+2.35, ML+1.3,
252 DV -2.5) of female mice at postnatal day 70-75. We performed behavior experiments seven days
253 after the injection and sacrificed the mice to confirm PNN degradation by histology. To stain the
254 PNN in the brain slice containing the OFC_L, we treated the fluorescein (FITC)-conjugated Wisteria
255 Floribunda Lectin (WFA, WFL) (Vector labs, cat#FL-1351) as a secondary antibody, diluted at
256 1:500 in 1X PBS, for 2 hours at RT before mounting the slices in a transparent mounting medium
257 (DAKO, cat#S3023). We manually and blindly counted the number of WFA^+ neurons within 0.5
258 x $0.5mm^2$ ROIs in three representative coronal sections covering OFC.

259 **CRISPR / Cas9 experiments**

260 *Generating the PX552-sgPV-tdTomato*

261 To generate the AAV-tdTomato vector, we first replaced the eGFP gene in PX552
262 (Addgene # 60958) with tdTomato. The tdTomato template was obtained from pAAV-FLEX-
263 tdTomato (Addgene # 28306). Next, we cloned two AAV-tdTomato plasmids, both of which
264 induce the targeted mutations at the parvalbumin gene (sgPV). One virus expresses two sgRNAs
265 targeting parvalbumin exon4: sgRNA1, 5'-AGACAAGTCTCTGGCATCTG-3' and sgRNA2, 5'-
266 AAGGATGGGGACGGCAAGAT-3' (Cloned recombinant DNA fragment:
267 AGACAAGTCTCTGGCATCTGGTTTTAGAGCTAGAAATAGCAAGTTAAAATAAGGCT
268 AGTCCGTTATCAACTTGAAAAAGTGGCACCGAGTCGGTGCAACAAAGCACCAGTGG
269 TCTAGTGGTAGAATAGTACCCTGCCACGGTACAGACCCGGGTTCGATTCCCGGCTGG
270 TGCAAAGGATGGGGACGGCAAGATGTTTTAGAGCTAGAAATAGCAAGTTAAAATAA
271 GGCTAGTCCGTTATCAACTTGAAAAAGTGGCACCGAGTCGGTGC, Bioneer & In-house
272 PCR amplification), and the other virus expresses two sgRNAs targeting parvalbumin exon5:
273 sgRNA3, 5'-GCTAAGTGGCGCTGACTGCT-3' and sgRNA4, 5'-
274 GGCCGCGAGAAGGACTGAGA-3'(Cloned recombinant DNA fragment:
275 GCTAAGTGGCGCTGACTGCTGTTTTAGAGCTAGAAATAGCAAGTTAAAATAAGGCT
276 AGTCCGTTATCAACTTGAAAAAGTGGCACCGAGTCGGTGCAACAAAGCACCAGTGG
277 TCTAGTGGTAGAATAGTACCCTGCCACGGTACAGACCCGGGTTCGATTCCCGGCTGG
278 TGCAGGCCGCGAGAAGGACTGAGAGTTTTAGAGCTAGAAATAGCAAGTTAAAATAA
279 GGCTAGTCCGTTATCAACTTGAAAAAGTGGCACCGAGTCGGTGC, Bioneer & In-house
280 PCR amplification).

281 After cloning the AAV-tdTomato vectors, we transfected them with packaging plasmid
282 into HEK293T (KCTC, cat# HC20005) to produce AAV-sgPV-tdTomato (exon4 and exon5) and

283 AAV-tdTomato, using lipofectamine 2000 (Invitrogen, cat# 11668-019). After 72hr, we collected
284 AAV (AAV2) particles from the cell lysates and performed iodixanol gradient ultracentrifugation.
285 Next, we concentrated the viral particles with Amicon Ultra Centrifugal Filter (Millipore) and
286 quantified the concentration of viral particles by quantitative PCR (genome copies per ml; AAV-
287 tdTomato, 3.92×10^{14}; AAV-sgPV(exon4)-tdTomato, 3.07×10^{12}; AAV-sgPV(exon5)-tdTomato,
288 7.17×10^{12}).

289 *Validation of CRISPR/Cas9 in the Neuro2a cell*

290 To identify the efficiency of sgPV in knocking down the PV, we transfected cloned AAV
291 vectors with the Cas9-eGFP expressing vector (PX458) in the Neuro2a cells. After 72h, we
292 collected and sorted tdTomato/eGFP double-positive cells using BD FACSAria II (BD
293 Biosciences). Next, we purified genomic DNA from sorted cells and performed PCR to amplify
294 the target sites of the PV gene, adding the index sequence for sequencing. Last, we subjected the
295 samples to Miniseq (Illumina) and analyzed insertion and deletion frequencies using CRISPR
296 RGEN Tools (http://www.rgenome.net/).

297 *Behavior and physiological experiments with CRISPR/Cas9 mice*

298 To express Cas9 selectively in PV^+ neurons, we crossed the PV-Cre mice (JAX #008069)
299 with the Rosa26-floxed STOP-Cas9 knock-in mice (JAX # 024857). We injected AAV-tdTomato
300 (tdTom) or AAV-sgPV-tdTomato (sgPV) into the crossed mice (PV::Cas9) on the postnatal day
301 50-65. On postnatal days 78-85, we performed the behavior test and *in vivo* recording. To verify
302 whether the AAV expression knocked down the PV effectively, we collected brain samples of the
303 injected mice and performed immunohistochemistry as described above. We used a combination
304 of the primary (rabbit anti-PV for PV staining, goat anti-GFP for Cas9 staining) and the secondary

305 (Alexa Fluor 405 donkey anti-goat IgG and Alexa Fluor 647 donkey anti-rabbit IgG were used)
306 antibodies.

307 *Whole-cell patch-clamp recordings in brain slices*

308 For electrophysiology experiments, tdTom/sgPV-expressed brain samples were collected
309 from anesthetized PV::Cas9 mice with isoflurane (Terrell) and sliced (coronal, 300 μm thickness)
310 using a vibratome (Leica VT1200). Brain extraction and sectioning were conducted in ice-cold
311 dissection buffer containing (in mM) 212 sucrose, 25 $NaHCO_3$, 5 KCl, 1.25 NaH_2PO_4, 0.5 $CaCl_2$,
312 3.5 $MgSO_4$, 10 D-glucose, 1.25 L-ascorbic acid and 2 Na-pyruvate bubbled with 95% O_2/5% CO_2.
313 The sectioned slices were incubated in a recovery chamber at 32 °C with normal ACSF (in mM:
314 125 NaCl, 2.5 KCl, 1.25 NaH_2PO_4, 25 $NaHCO_3$, 10 glucose, 2.5 $CaCl_2$ and 1.3 $MgCl_2$, oxygenated
315 with 95% O_2/5% CO_2). After 60-min recovery at 32 °C, slices were incubated for 30 min at room
316 temperature (20–25 °C). The slice was transferred to a recording chamber at 27–29 °C with
317 circulating ACSF saturated with 95% O_2 and 5% CO_2. Recording pipettes were made from thin-
318 walled borosilicate capillaries (30–0065, Harvard Apparatus) with resistance 3.0–4.0 MΩ using a
319 two-step vertical puller (PC-10, Narishege).

320 Whole-cell patch-clamp recordings were conducted using a MultiClamp 700B amplifier
321 (Molecular Devices) and Digidata 1550 (Molecular Devices). We recorded both AAV-expressed
322 and non-expressed neurons in the OFC_L. We confirmed the AAV expression by imaging the red
323 fluorescence of the patched cells under the fluorescent microscope (Olympus). During the
324 recordings, hyperpolarizing step pulses (5mV, 40ms) were injected into the cell to monitor
325 membrane resistance calculated by the peak amplitude of the capacitance current. Data from cells
326 that changed the resistance by more than 20% were excluded. To measure the intrinsic excitability,
327 recording pipettes (3.0–4.0MΩ) were filled with an internal solution containing (in mM) 137 K-

328 gluconate, 5 KCl, 10 HEPES, 0.2 EGTA, 10 Na-phosphocreatine, 4 Mg-ATP, and 0.5 Na-GTP,
329 with pH 7.2, 280 mOsm. Picrotoxin (Sigma, 100μM), NBQX (Tocris, 10μM), and D-AP5 (Tocris,
330 50μM) were added to ACSF to inhibit postsynaptic responses. After gigaseal and rupture, currents
331 were clamped, and RMP was maintained at -70mV. To measure the I-V curve, current inputs were
332 increased from -300 to 120pA in increments of 30pA per sweep with a time interval of 2 seconds.
333 To measure the I-F curve, current inputs were increased from 0 to 660pA in increments of 60pA
334 per sweep with a time interval of 10 seconds. For measuring sEPSCs in the OFC PV^+ neurons,
335 glass pipettes were filled with an internal solution composed of (in mM) 100 $CsMeSO_4$, 10 TEA-
336 Cl, 8 NaCl, 10 HEPES, 5 QX-314-Cl, 2 Mg-ATP, 0.3 Na-GTP, and 10 EGTA, with pH 7.25, 295
337 mOsm at a holding potential of -70 mV. Picrotoxin (100μM) was added to ACSF to block IPSCs.
338 For measuring sIPSCs in the OFC excitatory neurons, recording pipettes were filled with an
339 internal solution containing (in mM) 120 CsCl, 10 TEA-Cl, 8 NaCl, 10 HEPES, 5 QX-314-Cl, 4
340 Mg-ATP, 0.3 Na-GTP, and 10 EGTA, with pH 7.35, 280 mOsm holding at -70 mV. Circulating
341 ACSF were added NBQX and D-AP5 to block EPSCs. Data were acquired by Clampex 10.2
342 (Molecular Devices) and analyzed by Clampfit 10 (Molecular Devices).

343 **Wireless optogenetic modulation of the OFC neurons *in vivo***

344 *Design and fabrication of flexible optoelectronic neural probes*

345 Flexible optoelectronic probes were designed using electronic design automation software
346 (Altium Designer 18.0, Altium Limited) and produced using a conventional photolithography
347 process. Neural probes (0.1 mm thick) were designed in a bilateral form, in which the right and
348 the left probes (0.38 mm wide and 4 mm long each) were separated by 2.6 mm, to access both
349 regions of the mouse brain. Copper traces and electrodes (18 μm-thick) were patterned on one side
350 (i.e., top layer) of the polyimide substrate (25 μm-thick). In contrast, the other side (i.e., the bottom

351 layer) was covered with a copper layer (18 μm-thick) to stiffen the probe for penetration into brain
352 tissue. The probe tip part, where the microscale inorganic light-emitting diodes (μ-ILEDs;
353 TR2227, Cree; blue (473 nm) or green (532 nm), 270 × 220 × 50 μm^3) were attached, was not
354 covered with a copper layer to allow light emission from both sides of the probe. The fabricated
355 probes showed an optical intensity of ~405 mW/mm^2 at the top layer and ~45.3 mW/mm^2 at the
356 bottom layer, which sufficiently exceeds the threshold intensity for ChR2 activation (~1
357 mW/mm^2). A 3-pin plug-n-play female pin connector (M50-3130345, Harwin) and two μ-ILEDs
358 were mounted on the top layer electrodes after applying a low-temperature solder paste
359 (SMDLTLFP10T5, Chip Quik Inc.) and soldered using a precision soldering iron (NASE-2C, JBC
360 Soldering Tools) with the temperature of 250 °C. After confirming that every component was
361 robustly attached, probes were coated with Parylene C (7 μm-thick) for waterproofing. Lastly, the
362 probes were vertically bent and attached to a 3D-printed probe holder, followed by fixing them in
363 place using epoxy (5 Minute Epoxy, Permatex).

364 *Design of programmable wireless control module with detachable configuration*

365 A Bluetooth Low Energy (BLE) based wireless control module was designed to be easily
366 attached and detached with a bilateral optoelectronic probe and a battery through a plug-n-play
367 connection ((Qazi et al., 2019; Lee et al., 2020). This module controls the optical output of the μ-
368 ILEDs through smartphone manipulation. The electronic circuit of the wireless module consists of
369 a rechargeable Lithium Polymer (LiPo) battery (GM300910-PCB, PowerStream Technology; 12
370 mAh, 9 × 10 × 3 mm^3), a BLE System-on-Chip (SoC; EYSHSNZWZ, Taiyo Yuden; 8.55 × 3.25
371 × 0.3 mm^3), and various other electronic components (a linear voltage regulator, four decoupling
372 capacitors, two resistors, and two indicator LEDs). The current supplied from the LiPo battery is
373 regulated and stabilized by a voltage regulator (NCP4624DMU30TCG, onsemi) and decoupling

374 capacitors and flows to the BLE SoC to operate the module. Two indicator LEDs (VAOL-S4RP4,
375 VCC; red (624 nm wavelength)) were placed at the output pins of BLE SoC, each connected in
376 series with a resistor (RK73H1HTTC6041F, KOA Speer; 6.04 kΩ), to visually show the current
377 operation status of the module during the animal experiment – for example, the indicator LED
378 blinks every 5 seconds during optical stimulation. The wireless control module can be assembled
379 with optoelectronic probes through 3-pin plug-n-play connectors (male: M50-3630342, Harwin;
380 female: M50-3130345, Harwin) and assembled with LiPo battery through 2-pin connectors (male:
381 M50-3630242, Harwin; female: M50-3130245, Harwin). Every component except the LiPo
382 battery was soldered on the wireless module flexible printed circuit board (FPCB) of the wireless
383 module ($9.3 \times 7.6 \times 0.1$ mm^3), which was designed and manufactured through the same method
384 for the μ-ILED probes. The module was wirelessly programmed over the air (OTA; Nordic Device
385 Firmware Update (DFU) bootloader) to provide a pulse (20 Hz with 25 ms pulse width; i.e., 50%
386 duty cycle) or continuous (i.e., 100% duty cycle) current to the connected bilateral μ-ILED probes.
387 The BLE-based smartphone app was developed using commercial app development software
388 (Android Studio) and used to control the μ-ILED probes for wireless optogenetics.

389 *Virus injection and probe implantation surgery*

390 For optogenetic activation of excitatory neurons in the left OFC, we injected the AAV2-
391 CAMKIIα-eYFP (vector biolabs, VB1941) or AAV2-CAMKIIα-ChR2-eYFP (Addgene) virus in
392 the OFC_L (AP+2.35, ML±1.3, DV -2.5) of female WT mice between P50 to P60. For optogenetic
393 inactivation of PV^+ neurons in the left OFC, we injected the AAV9-EF1α-DIO-eYFP (UNC vector
394 core) or AAV9-EF1α-DIO-eArch3.0-eYFP (UNC vector core) virus in the OFC_L of female PV-
395 Cre transgenic mice. For the injection, we anesthetized mice using 1.5% isoflurane in oxygen
396 inhalation and performed stereotaxic surgery. Each injection contained 400nl of AAV- infused at

397 a rate of 0.4 nl/sec using a microinjector. We recovered the mice for 7 days after the AAV injection
398 and anesthetized mice again to implant the wireless optogenetic LED probe into the virus-
399 expressing OFC area. Because of the thickness of the probe (0.1mm) and the location of the LED
400 on the probe (+0.22 mm from the tip), we implanted the probe into the anterior and ventral part of
401 the OFC (AP +2.45, ML ±1.3, DV -2.77) to target the LED facing the virus-expressing area
402 without any lesion in it.

403 *Behavior test*

404 To connect the small module part to the implanted probe on the mouse head, we briefly
405 anesthetized the mice by isoflurane inhalation. After the module was connected, the mice had 10
406 min recovery phase in their home cage. On Day0, we habituated mice wearing a module for 15
407 min in the open field chamber. On Day1, we habituated the mice wearing a module in the
408 sociability chamber for 5 min. We then presented a novel social target and a novel object for 5 min
409 and recorded their approaching behaviors to measure the sociability of the mice. On Day2, we
410 performed a sociability test with blue or green LED stimulation for optogenetic modulation. We
411 gave 20Hz blue light stimulation by 473nm LED for activation or continuous green light
412 stimulation by 532nm LED for inactivation. The LED connected to the probe during the 5 min
413 sociability test session using the custom-designed flexible optoelectronic neural probes.
414 Interaction times of mice were analyzed on Day1 and Day2 as described previously. On Day3, we
415 performed an open field test for 5 min with optogenetic stimulation and 5 min without stimulation
416 to measure the effect of light activation on the locomotion behavior. After the behavior test, we
417 performed the histology of the brain samples from the mice to check the virus expression and probe
418 implanted site. We collected data only if the virus was expressed more than 65% of the total
419 volume of the OFC and the probe was targeted at the virus-expressed area.

420 **Experimental design & Statistical analysis**

421 All statistical analyses were performed using custom codes in IBM SPSS statistics 21 (IBM)
422 and OriginPro 2019 (Origin). The normal distribution of data was verified using the Shapiro-Wilk
423 normality test. For parametric tests, we used the paired student's t-test to compare matched pairs,
424 unpaired student's t-test to compare two groups, the one-way ANOVA with Fisher's least
425 significant difference [LSD] post hoc test to compare multiple groups, and two-way ANOVA test
426 to compare I-F curves of PV^+ neurons. For nonparametric tests, we used the Wilcoxon signed-rank
427 test to compare matched pairs, the Mann-Whitney *U* test to compare between two independent
428 groups, and the Kolmogorov–Smirnov test to compare the distributions of two groups. The number
429 of animals analyzed by statistical tests and the exact p values from each experiment were reported
430 within each figure legend.

431

Results

Post-weaning social isolation enhances sociability in female mice

Previous reports have shown that both short- and long-term social isolation affects mouse social behaviors (Makinodan et al., 2012; Matthews et al., 2016). However, the effects differ depending on the duration of isolation, and the data were collected only in male mice. To examine whether short- and long-term social isolation effects on mouse sociability differ between the sexes, we performed the sociability test in both male and female mice. For the sociability test, we put two small chambers at diagonal corners in the maze, each of which contained a novel object (O) or a novel and sex-matched mouse (M), and measured the relative times of mice sniffing or spending at or nearby the novel mouse compared to those times at the novel object as indices of the mouse sociability. We quantified the sociability in mice that had experienced three different post-weaning social conditions at postnatal day 80 (P80): group-housed (GH), socially isolated for one day (1dSI), or socially isolated for 60-days after weaning (post-weaning social isolation, PWSI) (Fig. 1A and 1B). Both the sniffing time of 1dSI mice when they came into contact with a novel mouse and their time spent in the social interaction zone did not differ significantly from those of GH mice in both males and females (Fig. 1C and 1D).

Notably, PWSI induced changes in sociability in a sex-specific manner: only female mice showed a significant increase in social sniffing time and social interaction time, while PWSI male mice showed normal sociability as the GH mice (Fig. 1C and 1D). We also confirmed that the effect of PWSI on female mice was not simply due to hormonal changes that occur during the estrous cycle. First, we confirmed that the estrous cycle was not different between GH and PWSI female mice (Fig. 1E). We next confirmed that the mouse sociability (both social sniffing index and social interaction index) that we measured was consistent across the estrous cycle in female

455 mice (Fig. 1F-1H). Therefore, our data indicate that long-term social isolation during adolescence
456 affects females' social behavior more than males, causing hypersociability in females.
457

458 **PWSI reduces PV expression in the OFC_L of female mice**

459 We next examined whether the social experience during adolescence is required to mature
460 PV^+ inhibitory circuits in the OFC. We quantified the number of PV^+ or PNN^+ neurons in the OFC
461 of the GH and the PWSI mice at P80. We collected data from male and female mice separately.
462 We first immunostained both for the PV, a marker for fast-spiking GABAergic neurons, and the
463 NeuN, a marker for all neurons (Fig. 2A). We counted the number of immunostained neurons
464 automatically in the three coronal sections that were collected across the center of the OFC (+2.1
465 ~ +2.34 mm from the bregma) per each hemisphere in each mouse (See Methods; Fig. 2B and 2C).
466 Interestingly, the number of PV^+ and $NeuN^+$ neurons in the OFC was significantly lower in the
467 brains of PWSI female mice compared to the GH female mice, especially in the left hemisphere
468 (Fig. 2D-2F). In male mice, however, the number of PV^+ and $NeuN^+$ neurons was not significantly
469 different between GH and PWSI groups (Fig. 2D-2F). When we counted the number of PV^- and
470 $NeuN^+$ neurons by subtracting the number of PV^+ neurons from the total number of $NeuN^+$ neurons,
471 there was no difference between groups (Fig. 3F; filled bars; female, OFC_L, p=1, Mann Whitney
472 U test). These data indicate that the reduction of $NeuN^+$ neurons preferentially occurs in the PV^+
473 neurons rather than in overall PV^- neurons in the OFC_L (Fig. 2F). We next quantified the PNN^+
474 neurons in the OFC by staining for *Wisteria floribunda agglutinin* (WFA), a marker for PNNs (Fig.
475 2G). Both PV^+ and PV^- neurons were surrounded by the PNNs in the OFC (Fig. 2H). We found
476 that the numbers of WFA^+ neurons in the OFC were not different between GH and PWSI in both
477 male and female mice (Fig. 2I). Collectively, our data indicate that social experience during

478 adolescence is crucial for the maturation of PV^+ neurons, especially the PV expression, in the
479 OFC_L of female mice.
480
481 **Late adolescence is a critical window for maturing sociability in female mice**
482 PWSI mice experienced long-term social isolation from when they were weaned at P21 to
483 when they became adults at P80. This period includes both early juvenile periods before the onset
484 of puberty and late adolescence after the onset of puberty. Since puberty leads to sexually
485 dimorphic changes in behaviors, we wondered how mouse sociability matures after the onset of
486 puberty in males and females. We thus tracked sociability changes from P50 (late adolescence
487 (Laviola et al., 2003) to P80 (adult) in both sexes of GH mice by measuring the social sniffing
488 index at P50 and at P80. Interestingly, we found a significant decrease in sociability at P80 in
489 female mice but not in male mice (Fig. 3A). We further found that during this period, PV^+ neurons
490 increased significantly in female OFC_L. In contrast, OFC_R did not show such an increase between
491 P50 and P80 period (Fig. 3B). These data suggest that late adolescence from P50 to P80 is a critical
492 window for the maturation of sociability with an increase in PV^+ neurons in the OFC_L in female
493 mice.
494 We next examined the effect of social isolation during late adolescence in both female and
495 male mice. We directly isolated the mice after P50 until P80 (P50SI; Fig. 3C). In addition, we re-
496 group-housed a group of PWSI female mice at P50 to make them re-experience social interaction
497 during late adolescence (re-GH; Fig. 3C). The P50SI female mice showed an increase in sociability
498 like the PWSI female mice, while reGH female mice nor P50SI male mice did not show any
499 changes in sociability compared to control GH mice (Fig. 3D). Not only our modified 3-chamber-
500 like test, but a standard 3-chamber test also showed an increase in sociability in P50SI female mice

501 (data not shown). In addition, the number of PV^+ neurons in re-GH female mice was not
502 significantly different from that in GH female mice in both hemispheres of the OFC (Fig. 3E),
503 indicating that social experience during late adolescence was sufficient to mature the PV^+ neurons
504 in the OFC_L.

505 Finally, we wondered whether the enhanced sociability in P50SI female mice, measured
506 by our sociability test, was related with changes in aggression. To examine this, we performed the
507 resident-intruder test (Tan et al., 2021) on P50SI male and female mice. We counted both offensive
508 behaviors, such as threatening and attacking behaviors, and social behaviors, such as nose sniffing
509 and anogenital sniffing, separately during the test (Fig.3F). In female mice, the aggression level
510 did not increase by P50SI. Still, the social approaching behaviors significantly increased (Fig. 3G).
511 On the other hand, P50SI male mice showed a significant increase in aggression without any
512 changes in social behaviors (Fig. 3H). Collectively, our data indicate that social isolation during
513 late adolescence induced hypersociability in female mice without increasing aggression whereas
514 it induced hyperaggression in male mice.

515

516 **PWSI disrupts social sniffing-induced activity in the OFC_L of female mice**

517 Because PV^+ neurons in the OFC_L were found to be less numbered following PWSI in
518 female mice, we investigated whether the OFC_L neural response to social contact has been altered
519 in head-fixed female mice by *in vivo* multichannel recordings (Fig. 4A and 4B). During the
520 recording, both GH and PWSI female mice showed sniffing behaviors toward an object or another
521 mouse under the head-fixed condition, and the number and duration of sniffing times did not differ
522 between groups (Fig. 4C and 4D). We identified neurons that showed significant sniffing-induced
523 activity in the OFC (Fig. 4E-4H). Interestingly, in GH females, more neurons showed sniffing-

524 induced activity in the OFC_L than in the OFC_R responses, and their responses were stronger when
525 a mouse sniffed another mouse than when it sniffed an object (Fig. 4E and 4F). More importantly,
526 these socially responsive neurons in the OFC_L of female mice largely disappeared after PWSI (Fig.
527 4E, 4G, and 4H). On the other hand, the sniffing-induced activity of the OFC_R did not differ
528 between GH and PWSI female mice (Fig. 4F). Among the responsive neurons in the OFC_L, the
529 fraction of the fast-spiking neurons was smaller in the PWSI mice than in the GH mice. These data
530 indicate that PWSI decreased social sniffing-induced activity in the OFC_L neurons, particularly
531 including fast-spiking neurons, and reduced overall social representation in the OFC_L.

532

533 **PV^+ expression, not PNNs in the OFC_L, shapes social behavior in female mice**

534 As we found that PWSI impaired the PV expression in the OFC_L and increased social
535 behavior, we next examined the causal relationship between the reduction of PV expression in the
536 OFC_L and the increase in the sociability of female mice. To reduce the PV expression *in vivo*, we
537 used the CRISPR/Cas9 system (Swiech et al., 2015) and designed two pairs of single-guide RNAs
538 (sgRNAs) to target the 4th and 5th exons of the PV gene (sgPV). We first confirmed that those
539 sgRNAs knocked out the PV gene by either deletion or insertion of the targeted sequences in more
540 than 85% of the Cas9-transfected Neuro2a cells (Fig. 5A). We then constructed the adeno-
541 associated viral vectors (AAVs) to deliver those sgRNAs together with the tdTomato gene to
542 neurons *in vivo* (Fig. 5A) and injected the AAVs into the cortex of PV::Cas9-eGFP mice, which
543 were created by crossing PV-Cre with $Cas9^{fl/fl}$-eGFP mice (sgPV; and Fig. 5B-C). As a control,
544 we injected the AAV that expressed only the tdTomato without sgRNAs into the crossed mice
545 (tdTom). In the sgPV mice, originally PV^+ neurons were expressed with both Cas9-eGFP and

546 tdTomato, and their PV gene was knocked out by Cas9 in the PV^+ neurons selectively (Fig. 5B-
547 C).

548 To knock down PV in the OFC_L during late adolescence until mice became adults, we
549 injected the AAVs into the OFC_L when mice were at around P50 and examined changes in the
550 sociability of the injected mice at P80. We confirmed the reduction of PV expression in the
551 $eGFP^+$/$tdTomato^+$ neurons without any decrease in PNN expression by immunostaining the PV
552 and the PNNs in the OFC_L (Fig. 5D-E). The female mice with PV knock-down in the OFC_L showed
553 a significant increase in sociability (Fig. 5H), similar to the PWSI or P50SI females (Fig. 1B-1D
554 and Fig. 3D). When we knocked down the PV in the OFC_R of female mice or the OFC_L of male
555 mice, we did not see such an increase in sociability compared to the control mice (Fig. 5H). We
556 further examined whether a reduction in PNNs surrounding PV^+ neurons affects female sociability.
557 We infused chondroitinase ABC (chABC), an enzyme that degrades PNNs by removing sulfate
558 side chains of proteoglycans, into the OFC_L (Fig. 5F). Treatment with chABC significantly
559 decreased the number of WFA^+ neurons in the OFC_L without affecting PV expression (Fig. 5G).
560 Not like the female mice knocked down with PV, the female mice treated with chABC showed
561 normal sociability (Fig. 5I). Together, our data indicate that the PV expression, but not the PNN
562 maturation, in the OFC_L was a key factor shaping the social behavior of female mice.

563

564 **Decreased PV expression reduces social sniffing-induced activity via hyper-excitation of**
565 **OFC_L neurons**

566 We next investigated whether the decrease of PV expression in the OFC_L was responsible
567 for the reduced sniffing-induced activity in the OFC_L of the PWSI female mice. We performed *in*
568 *vivo* recordings in female mice injected with sgPV AAVs (**sgPV**) or injected with tdTomato AAVs

569 (**tdTom**) in their OFC_L (Fig. 6A-6G). First, we found that the average baseline firing rates were
570 significantly higher in the spPV group compared to the tdTom group (Fig. 6D and 6E).
571 Furthermore, similar to PWSI, knocking down PV by sgPV decreased social sniffing-induced
572 activity in the OFC_L of female mice (**sgPV**; Fig. 6F and 6G). Conversely, the expression of
573 tdTomato in the OFC_L did not alter the sniffing-induced activity of female mice (**tdTom**; Fig. 6F
574 and 6G). Knocking down PV in the OFC_L did not affect the sniffing behavior itself, as the number
575 and duration of sniffs in the altered mice were similar to those in the tdTom control mice (Fig. 6C).
576 These data indicate that the knock-down of PV increased overall firing activity while reducing the
577 sniffing-induced activity in the OFC_L.

578 As we observed an increase in the baseline activity of OFC_L neurons by knocking down
579 the PV, we next examined whether the knock-down of PV has altered the excitation-inhibition
580 balance in the OFC_L of female mice. We first performed patch-clamp recordings of the PV^+
581 neurons in the OFC_L by targeting $tdTomato^+$ neurons of PV::Cas9 mice injected with sgPV or
582 tdTom AAVs into the OFC_L (Fig. 6H-6L). We found that the knock-out of the PV gene by sgPV
583 in PV^+ neurons reduced the intrinsic excitability of those neurons (Fig. 6I) without any changes in
584 spontaneous excitatory synaptic currents (sEPSCs; Fig. 6L). Other membrane properties, such as
585 the half-width of spike waveforms and the input resistance, were normal in those neurons (Fig. 6J
586 and 6K). We next measured the spontaneous inhibitory postsynaptic currents (sIPSCs) in the OFC_L
587 neurons, which were not labeled with the tdTomato in the sgPV and the tdTom mice. These
588 neurons were regular spiking and thus putative excitatory neurons in the OFC_L (Fig. 6H and 6M).
589 The OFC_L excitatory neurons in the sgPV mice showed a significant decrease in both amplitudes
590 and frequencies of spontaneous IPSCs compared to the tdTom control mice (Fig. 6M). These data

591 indicate that the decreased expression of PV in the OFC_L reduced the excitability of the PV^+
592 neurons and, in turn, reduced inhibition of the neighboring neurons in the OFC_L of female mice.
593 Our recording data suggested that the decrease in inhibition upon knocking down the PV
594 gene caused an increase in excitation, which led to a rise in the baseline activity of OFC_L and
595 disruption in sniffing-induced activities (Fig. 6D-6G). We thus examined whether the abnormal
596 increase of OFC_L activity caused hypersociability in female mice. We expressed the
597 channelrhodopsin-2 (ChR2) in the excitatory neurons of the OFC_L by injecting the AAV virus,
598 which expresses the ChR2 fused to the eYFP under the CaMKIIα promotor, to the wild-type
599 female mice (Fig. 7A and 7C). We then delivered the light stimulation to the OFC_L by inserting a
600 wireless optogenetic device that we developed (Kim et al., 2021; Qazi et al., 2021) to provide the
601 20Hz blue lights during the sociability tests (Fig. 7B; see Methods). The stimulation was given on
602 the second day of the sociability tests. We measured the first-day sociability (Day1) without the
603 light stimulation and did not observe any differences in the sociability between the ChR2-eYFP
604 and the eYFP groups. We tested their sociability again on the second day with the blue-light
605 stimulation on the OFC_L (Day2). The eYFP control mice showed a significant decrease in their
606 sociability on Day2 compared to Day1, potentially due to habituation (Fig. 7D and E). On the other
607 hand, the ChR2-eYFP-expressed mice showed higher levels of social sniffing behaviors with light
608 stimulation than the control mice on Day2 (Fig. 7D). This data indicates that the optogenetic
609 activation of the OFC_L induced higher sociability and almost no habituation in social approaching
610 behaviors on Day2 (Fig. 7D and 7E). We next optogenetically inactivated the PV^+ neurons in
611 OFC_L directly during the sociability test on Day2 by expressing the Archaerhodopsin-3 (eArch3.0)
612 in PV^+ neurons and delivering 532nm light through our wireless probe (Fig. 7G). Similar to the
613 optogenetic activation of excitatory neurons in the OFC_L, inhibition of PV^+ neurons induced

614 hypersociability in female mice without habituation on Day 2, when we gave the light stimulation
615 in the OFC_L (Fig. 7H and 7I). The light stimulation did not affect the locomotion in both groups
616 (Fig. 7F and 7J). Collectively, our data demonstrate that hyper-excitation of the OFC_L by reducing
617 inhibition caused hypersociability in female mice.

618 **Discussion**

619 Our study found that adolescent social experience is critical for shaping sociability in
620 female mice. Social isolation during late adolescence enhanced sociability in female mice while
621 impairing the maturation of PV^+ neurons and decreasing social sniffing-induced activity in the
622 OFC_L. The knock-down of PV in the OFC_L of female mice induced the same phenotype as the
623 PWSI mice: enhanced sociability and decreased sniffing-induced activity in the OFC_L. These
624 effects were due to the imbalance between excitation and inhibition, as the PV knock-down caused
625 hyper-excitation in the OFC_L. We further found that optogenetic activation of excitatory neurons
626 or suppression of PV^+ inhibitory neurons in the OFC_L led to enhanced sociability in female mice.
627 This finding supports the idea that the excitation-inhibition balance in the prefrontal cortex is
628 critical for shaping social behaviors in mice (Yizhar et al., 2011). Our data also suggest that
629 adolescent social isolation influences male and female mice differently, both in how the prefrontal
630 cortex matures and social behavior matures.

631

632 **Importance of social experience during adolescence in shaping female social behavior**

633 Social experience during adolescence is important for the maturation of the mammalian
634 brain (Spear, 2000; Fuhrmann et al., 2015). In humans, social isolation during adolescence can
635 increase the occurrence of neurological disorders and cause defects in brain function (Almeida et
636 al., 2021). Similarly, depriving rodents of social experience during adolescence caused defects in
637 the maturation of their brains and alterations in social and cognitive behaviors (Cooke et al., 2000;
638 Schubert et al., 2009; Makinodan et al., 2012; Hinton et al., 2019; Potrebic et al., 2022).
639 Furthermore, behavioral and physiological changes caused by adolescent social isolation were
640 often sex-specific (Pisu et al., 2016; Bicks et al., 2020; Tan et al., 2021). In this study, we found

641 that PWSI, particularly after puberty (from P50 to P80), impairs the maturation of inhibitory
642 circuits in the OFC_L and causes maladaptation in social exploration behavior in female mice but
643 not in male mice. Our study is unique compared to recent studies that examined the effects of
644 social isolation during early adolescence (Bicks et al., 2020; Tan et al., 2021). Our findings
645 emphasize the importance of later adolescence when females adjust and shape their social
646 approaching behaviors with the maturation of PV^+ neurons in the OFC_L.

647 A recent study has shown that the 1dSI increased sociability in male mice (Matthews et al.,
648 2016). We also found that male mice that had experienced 1dSI spent more time interacting with
649 a novel mouse than did GH male mice (GH, 221.11 ± 17.93 s, 1dSI, 317.97 ± 31.46 s, p=0.023,
650 student's t-test). However, the 1dSI male mice also showed a tendency of increased interaction
651 with an object in the other container (GH, 107.29± 9.88 s, 1dSI, 138.28 ± 23.36 s, p=0.256,
652 student's t-test). As a result, their social sniffing and social interaction indices, which indicate the
653 ratio between social interaction and object interaction times, did not change in 1dSI male mice
654 (Fig. **1C** and **1D**). Our data suggest that 1dSI may enhance object exploration behaviors in male
655 mice. This possibility was not tested in the previous report, as they used an empty chamber without
656 any object as opposed to the social chamber. Future studies are required to understand the effect
657 of 1dSI in male mice fully. Regardless, our study focuses on the social isolation effect on female
658 mice, and we found no effects of 1dSI on social and object interaction times in female mice. Our
659 data demonstrate that long-term social isolation during late adolescence affects social behaviors
660 more effectively than the 1dSI in females.

661 PWSI not only deprives sensory experience from social interaction but also enhances stress
662 in social mammals like mice (Fone and Porkess, 2008). It has been shown that both sensory
663 deprivation and stress can impair the maturation of PV^+ neurons in the sensory cortex as well as

664 in the hippocampus (Huang et al., 1999; Czeh et al., 2005; Hu et al., 2010). The OFC, which is
665 classified as a secondary olfactory cortex, is one of the key areas involved in olfactory processing
666 (Lipton et al., 1999) and sniffing behaviors (Kareken et al., 2004). Furthermore, the olfactory
667 system is the most important way through which mice detect other mice (Radyushkin et al., 2009).
668 The OFC has a strong connection with the olfactory system and the hippocampus (Wikenheiser
669 and Schoenbaum, 2016). An fMRI study in humans showed that in response to odorant cues with
670 emotional valence, only females showed increased activity in their OFC_L (Royet et al., 2003).
671 Future studies are required to unravel which types of social olfactory cues and stress-related factors
672 affect the maturation of PV^+ neurons in the OFC_L and social behavior.

673 Our data suggest that socially evoked activity in the OFC_L is important for reducing social
674 approaching behaviors when the animal becomes an adult. Excessive sociability is a symptom of
675 patients with Williams-Beuren syndrome (Mimura et al., 2010; Sakurai et al., 2011; Segura-
676 Puimedon et al., 2014; Stoppel and Anderson, 2017) or Angelman syndrome (Stoppel and
677 Anderson, 2017; Simchi and Kaphzan, 2021), rare neurodevelopmental genetic disorders.
678 Interestingly, these patients show abnormal activity patterns in the OFC. Hypersociability is also
679 found in some mouse models of autism (Yoo et al., 2019). Our data demonstrate that PWSI induced
680 similar behavioral abnormalities in female mice, suggesting that the normal maturation and activity
681 of the OFC_L, at least in females, is important for maintaining an adequate level of sociability in
682 such disorders.

683

684 **PV expression in the OFC_L is important for female social behavior**

685 Recent studies found important roles of PV expression in the PFC in shaping social and
686 cognitive behaviors. For example, several mouse models of autism that show impaired sociability

687 have shown reduced PV expression in the mPFC (Filice et al., 2016; Kobayashi et al., 2018).
688 Furthermore, maternal separation before weaning (Goodwill et al., 2018) or social isolation during
689 early adolescence (Hinton et al., 2019) reduced PV expression in the OFC and impaired flexibility
690 in behavioral decisions in rodents. Whole-brain knock-out of PV caused the mice to show autism-
691 like behavior (Wohr et al., 2015), but it is still unclear whether the reduced PV expression in sub-
692 regions of the PFC caused such behavioral deficits. Our study newly applied the CRISPR/Cas9
693 system to reduce PV expression locally in the OFC_L. Using this method, we confirmed that PV
694 expression in the OFC_L during adolescence is critical for shaping social behaviors in female mice
695 (Fig. **5**). This technique can be widely used for studying area-specific PV protein function in
696 various brain areas, although it lacks the reversibility of the loss-of-function by permanent gene
697 deletion *in vivo*.

698 PV is a calcium-binding protein that plays a key role in regulating the physiological
699 properties of PV^+ neurons. In our study, knocking down PV decreased the excitability of the PV^+
700 inhibitory neurons, which in turn decreased synaptic inhibition on nearby excitatory neurons (Fig.
701 **6H-6M**). The relative reduction in inhibition compared to excitation in the OFC_L potentially
702 disrupted overall social sniffing-induced activity in the OFC_L (Fig. **6F** and **6G**) and
703 hypersociability (Fig. **5H**). We further proved this idea by the optogenetic activation of excitatory
704 neurons in the OFC_L that led to hypersociability (Fig. **7**). Moreover, a reduced number of PV^+
705 neurons can also disrupt the network property of the OFC_L, similar to the previous report showing
706 that the loss of PV^+ neurons correlated with a decrease in the network oscillation in the PFC (Lodge
707 et al., 2009). Maturation of network activity during adolescence may be critical for shaping social
708 sniffing-induced activity in the OFC_L.

709 In a study of virgin female mice, PV and PNN expression in the auditory cortex was
710 reported to be correlated with learning to retrieve pups (Krishnan et al., 2017); this activity, which
711 occurs in the left auditory cortex, is important for shaping maternal behaviors in female mice
712 (Marlin et al., 2015). Although several studies have shown that the expression of PNN is important
713 for the maturation of PV^+ neurons (Gogolla et al., 2009), we found expression of the PV but not
714 the PNN is important for the maturation of the female OFC_L during late adolescence. Our data
715 suggest that transcription or translation of PV and PNN may be separately regulated, and
716 adolescent social isolation specifically disrupted PV expression only in a subset of neurons in the
717 OFC_L. Our data further support the idea that plasticity in PV^+ neurons in the OFC_L is important
718 for shaping female sociability and is also characterized by hemispheric asymmetry. Both genetic
719 and epigenetic mechanisms have been identified as critical for regulating normal social behavior
720 (Hensch, 2005), and thus social behaviors can be easily disrupted in a wide range of brain
721 psychiatric disorders (Blakemore, 2008). Our study further provides insight into how disruption of
722 experience-dependent gene expression in the PFC inhibitory neurons, such as reduced PV
723 expression in the OFC_L, may underlie abnormal hypersociability that characterizes certain
724 psychiatric disorders.

725

726 **Contact for reagent and resource sharing**

727 Further information about and requests for reagents may be directed to and will be fulfilled
728 by the corresponding author, Dr. Seung-Hee Lee (shlee1@kaist.ac.kr).

729

730 **Author contributions**

YSJ and DJ performed most of the experiments and contributed equally to this work; HK and EK performed and evaluated patch-clamp recording experiments; JHK helped to perform *in vivo* recordings and measure sniffing behavior; CYK and JWJ designed and fabricated the wireless-controllable optoelectronic neural probes; YO and SGK designed and cloned the AAV-sgPV vectors; YHL and CHK cloned the AAV-tdTomato vectors; SHL designed and supervised the study. YSJ, DJ, SHL wrote the manuscript with contributions from all the authors.

References

Adolphs R (2003) Cognitive neuroscience of human social behaviour. Nat Rev Neurosci 4:165-178.

Almeida ILL, Rego JF, Teixeira ACG, Moreira MR (2021) Social isolation and its impact on child and adolescent development: a systematic review. Rev Paul Pediatr 40:e2020385.

Amodio DM, Frith CD (2006) Meeting of minds: the medial frontal cortex and social cognition. Nat Rev Neurosci 7:268-277.

Beurdeley M, Spatazza J, Lee HH, Sugiyama S, Bernard C, Di Nardo AA, Hensch TK, Prochiantz A (2012) Otx2 binding to perineuronal nets persistently regulates plasticity in the mature visual cortex. J Neurosci 32:9429-9437.

Bicks LK, Koike H, Akbarian S, Morishita H (2015) Prefrontal Cortex and Social Cognition in Mouse and Man. Front Psychol 6:1805.

Bicks LK, Yamamuro K, Flanigan ME, Kim JM, Kato D, Lucas EK, Koike H, Peng MS, Brady DM, Chandrasekaran S, Norman KJ, Smith MR, Clem RL, Russo SJ, Akbarian S, Morishita H (2020) Prefrontal parvalbumin interneurons require juvenile social experience to establish adult social behavior. Nat Commun 11:1003.

Blakemore SJ (2008) The social brain in adolescence. Nat Rev Neurosci 9:267-277.

Celio MR, Blumcke I (1994) Perineuronal nets--a specialized form of extracellular matrix in the adult nervous system. Brain Res Brain Res Rev 19:128-145.

Cheong RY, Tonetto S, von Horsten S, Petersen A (2020) Imbalance of the oxytocin-vasopressin system contributes to the neuropsychiatric phenotype in the BACHD mouse model of Huntington disease. Psychoneuroendocrinology 119:104773.

Cooke BM, Chowanadisai W, Breedlove SM (2000) Post-weaning social isolation of male rats reduces the volume of the medial amygdala and leads to deficits in adult sexual behavior. Behav Brain Res 117:107-113.

Czeh B, Simon M, van der Hart MG, Schmelting B, Hesselink MB, Fuchs E (2005) Chronic stress decreases the number of parvalbumin-immunoreactive interneurons in the hippocampus: prevention by treatment with a substance P receptor (NK1) antagonist. Neuropsychopharmacology 30:67-79.

Dityatev A, Bruckner G, Dityateva G, Grosche J, Kleene R, Schachner M (2007) Activity-dependent formation and functions of chondroitin sulfate-rich extracellular matrix of perineuronal nets. Dev Neurobiol 67:570-588.

Enwright JF, Sanapala S, Foglio A, Berry R, Fish KN, Lewis DA (2016) Reduced Labeling of Parvalbumin Neurons and Perineuronal Nets in the Dorsolateral Prefrontal Cortex of Subjects with Schizophrenia. Neuropsychopharmacology 41:2206-2214.

Filice F, Vorckel KJ, Sungur AO, Wohr M, Schwaller B (2016) Reduction in parvalbumin expression not loss of the parvalbumin-expressing GABA interneuron subpopulation in genetic parvalbumin and shank mouse models of autism. Mol Brain 9:10.

Fone KC, Porkess MV (2008) Behavioural and neurochemical effects of post-weaning social isolation in rodents-relevance to developmental neuropsychiatric disorders. Neurosci Biobehav Rev 32:1087-1102.

Franklin KBJ, Paxinos G The mouse brain in stereotaxic coordinates.

Fuhrmann D, Knoll LJ, Blakemore SJ (2015) Adolescence as a Sensitive Period of Brain Development. Trends Cogn Sci 19:558-566.

781 Gogolla N, Caroni P, Luthi A, Herry C (2009) Perineuronal nets protect fear memories from
782 erasure. Science 325:1258-1261.
783 Goodwill HL, Manzano-Nieves G, LaChance P, Teramoto S, Lin S, Lopez C, Stevenson RJ,
784 Theyel BB, Moore CI, Connors BW, Bath KG (2018) Early Life Stress Drives Sex-
785 Selective Impairment in Reversal Learning by Affecting Parvalbumin Interneurons in
786 Orbitofrontal Cortex of Mice. Cell Rep 25:2299-2307 e2294.
787 Grishagin IV (2015) Automatic cell counting with ImageJ. Anal Biochem 473:63-65.
788 Hazan L, Zugaro M, Buzsaki G (2006) Klusters, NeuroScope, NDManager: a free software suite
789 for neurophysiological data processing and visualization. J Neurosci Methods 155:207-
790 216.
791 Hensch TK (2005) Critical period plasticity in local cortical circuits. Nat Rev Neurosci 6:877-
792 888.
793 Hinton EA, Li DC, Allen AG, Gourley SL (2019) Social Isolation in Adolescence Disrupts
794 Cortical Development and Goal-Dependent Decision-Making in Adulthood, Despite
795 Social Reintegration. eNeuro 6.
796 Hu W, Zhang M, Czeh B, Flugge G, Zhang W (2010) Stress impairs GABAergic network
797 function in the hippocampus by activating nongenomic glucocorticoid receptors and
798 affecting the integrity of the parvalbumin-expressing neuronal network.
799 Neuropsychopharmacology 35:1693-1707.
800 Huang ZJ, Kirkwood A, Pizzorusso T, Porciatti V, Morales B, Bear MF, Maffei L, Tonegawa S
801 (1999) BDNF regulates the maturation of inhibition and the critical period of plasticity in
802 mouse visual cortex. Cell 98:739-755.
803 Kareken DA, Sabri M, Radnovich AJ, Claus E, Foresman B, Hector D, Hutchins GD (2004)
804 Olfactory system activation from sniffing: effects in piriform and orbitofrontal cortex.
805 Neuroimage 22:456-465.
806 Kim CY, Ku MJ, Qazi R, Nam HJ, Park JW, Nam KS, Oh S, Kang I, Jang JH, Kim WY, Kim
807 JH, Jeong JW (2021) Soft subdermal implant capable of wireless battery charging and
808 programmable controls for applications in optogenetics. Nat Commun 12:535.
809 Kobayashi M, Hayashi Y, Fujimoto Y, Matsuoka I (2018) Decreased parvalbumin and
810 somatostatin neurons in medial prefrontal cortex in BRINP1-KO mice. Neurosci Lett
811 683:82-88.
812 Krishnan K, Lau BY, Ewall G, Huang ZJ, Shea SD (2017) MECP2 regulates cortical plasticity
813 underlying a learned behaviour in adult female mice. Nat Commun 8:14077.
814 Laviola G, Macri S, Morley-Fletcher S, Adriani W (2003) Risk-taking behavior in adolescent
815 mice: psychobiological determinants and early epigenetic influence. Neurosci Biobehav
816 Rev 27:19-31.
817 Lee E, Hong J, Park YG, Chae S, Kim Y, Kim D (2015) Left brain cortical activity modulates
818 stress effects on social behavior. Sci Rep 5:13342.
819 Lee J, Parker KE, Kawakami C, Kim JR, Qazi R, Yea J, Zhang S, Kim CY, Bilbily J, Xiao J,
820 Jang KI, McCall JG, Jeong JW (2020) Rapidly-customizable, scalable 3D-printed
821 wireless optogenetic probes for versatile applications in neuroscience. Adv Funct Mater
822 30.
823 Lipton PA, Alvarez P, Eichenbaum H (1999) Crossmodal associative memory representations in
824 rodent orbitofrontal cortex. Neuron 22:349-359.

825 Lodge DJ, Behrens MM, Grace AA (2009) A loss of parvalbumin-containing interneurons is
826 associated with diminished oscillatory activity in an animal model of schizophrenia. J
827 Neurosci 29:2344-2354.
828 Luhmann HJ, Prince DA (1991) Postnatal maturation of the GABAergic system in rat neocortex.
829 J Neurophysiol 65:247-263.
830 Makinodan M, Rosen KM, Ito S, Corfas G (2012) A critical period for social experience-
831 dependent oligodendrocyte maturation and myelination. Science 337:1357-1360.
832 Marlin BJ, Mitre M, D'Amour J A, Chao MV, Froemke RC (2015) Oxytocin enables maternal
833 behaviour by balancing cortical inhibition. Nature 520:499-504.
834 Matthews GA, Nieh EH, Vander Weele CM, Halbert SA, Pradhan RV, Yosafat AS, Glober GF,
835 Izadmehr EM, Thomas RE, Lacy GD, Wildes CP, Ungless MA, Tye KM (2016) Dorsal
836 Raphe Dopamine Neurons Represent the Experience of Social Isolation. Cell 164:617-
837 631.
838 McLean AC, Valenzuela N, Fai S, Bennett SA (2012) Performing vaginal lavage, crystal violet
839 staining, and vaginal cytological evaluation for mouse estrous cycle staging
840 identification. J Vis Exp:e4389.
841 Mimura M, Hoeft F, Kato M, Kobayashi N, Sheau K, Piggot J, Mills D, Galaburda A, Korenberg
842 JR, Bellugi U, Reiss AL (2010) A preliminary study of orbitofrontal activation and
843 hypersociability in Williams Syndrome. J Neurodev Disord 2:93-98.
844 Murugan M, Jang HJ, Park M, Miller EM, Cox J, Taliaferro JP, Parker NF, Bhave V, Hur H,
845 Liang Y, Nectow AR, Pillow JW, Witten IB (2017) Combined Social and Spatial Coding
846 in a Descending Projection from the Prefrontal Cortex. Cell 171:1663-1677 e1616.
847 Nakanishi M, Nomura J, Ji X, Tamada K, Arai T, Takahashi E, Bucan M, Takumi T (2017)
848 Functional significance of rare neuroligin 1 variants found in autism. PLoS Genet
849 13:e1006940.
850 Paus T, Keshavan M, Giedd JN (2008) Why do many psychiatric disorders emerge during
851 adolescence? Nat Rev Neurosci 9:947-957.
852 Pisu MG, Garau A, Boero G, Biggio F, Pibiri V, Dore R, Locci V, Paci E, Porcu P, Serra M
853 (2016) Sex differences in the outcome of juvenile social isolation on HPA axis function
854 in rats. Neuroscience 320:172-182.
855 Potrebic M, Pavkovic Z, Puskas N, Pesic V (2022) The Influence of Social Isolation on Social
856 Orientation, Sociability, Social Novelty Preference, and Hippocampal Parvalbumin-
857 Expressing Interneurons in Peripubertal Rats - Understanding the Importance of Meeting
858 Social Needs in Adolescence. Front Behav Neurosci 16:872628.
859 Qazi R, Gomez AM, Castro DC, Zou Z, Sim JY, Xiong Y, Abdo J, Kim CY, Anderson A,
860 Lohner F, Byun SH, Chul Lee B, Jang KI, Xiao J, Bruchas MR, Jeong JW (2019)
861 Wireless optofluidic brain probes for chronic neuropharmacology and photostimulation.
862 Nat Biomed Eng 3:655-669.
863 Qazi R, Parker KE, Kim CY, Rill R, Norris MR, Chung J, Bilbily J, Kim JR, Walicki MC,
864 Gereau GB, Lim H, Xiong Y, Lee JR, Tapia MA, Kravitz AV, Will MJ, Ha S, McCall
865 JG, Jeong JW (2021) Scalable and modular wireless-network infrastructure for large-
866 scale behavioural neuroscience. Nat Biomed Eng.
867 Radyushkin K, Hammerschmidt K, Boretius S, Varoqueaux F, El-Kordi A, Ronnenberg A,
868 Winter D, Frahm J, Fischer J, Brose N, Ehrenreich H (2009) Neuroligin-3-deficient mice:
869 model of a monogenic heritable form of autism with an olfactory deficit. Genes Brain
870 Behav 8:416-425.

871 Royet JP, Plailly J, Delon-Martin C, Kareken DA, Segebarth C (2003) fMRI of emotional
872 responses to odors: influence of hedonic valence and judgment, handedness, and gender.
873 Neuroimage 20:713-728.
874 Rudy B, Fishell G, Lee S, Hjerling-Leffler J (2011) Three groups of interneurons account for
875 nearly 100% of neocortical GABAergic neurons. Dev Neurobiol 71:45-61.
876 Sakurai T, Dorr NP, Takahashi N, McInnes LA, Elder GA, Buxbaum JD (2011)
877 Haploinsufficiency of Gtf2i, a Gene Deleted in Williams Syndrome, Leads to Increases in
878 Social Interactions. Autism Res 4:28-39.
879 Schubert MI, Porkess MV, Dashdorj N, Fone KC, Auer DP (2009) Effects of social isolation
880 rearing on the limbic brain: a combined behavioral and magnetic resonance imaging
881 volumetry study in rats. Neuroscience 159:21-30.
882 Segura-Puimedon M, Sahun I, Velot E, Dubus P, Borralleras C, Rodrigues AJ, Valero MC,
883 Valverde O, Sousa N, Herault Y, Dierssen M, Perez-Jurado LA, Campuzano V (2014)
884 Heterozygous deletion of the Williams-Beuren syndrome critical interval in mice
885 recapitulates most features of the human disorder. Hum Mol Genet 23:6481-6494.
886 Simchi L, Kaphzan H (2021) Aberrant aggressive behavior in a mouse model of Angelman
887 syndrome. Sci Rep-Uk 11.
888 Spear LP (2000) The adolescent brain and age-related behavioral manifestations. Neurosci
889 Biobehav Rev 24:417-463.
890 Stoppel DC, Anderson MP (2017) Hypersociability in the Angelman syndrome mouse model.
891 Exp Neurol 293:137-143.
892 Sugiyama S, Di Nardo AA, Aizawa S, Matsuo I, Volovitch M, Prochiantz A, Hensch TK (2008)
893 Experience-dependent transfer of Otx2 homeoprotein into the visual cortex activates
894 postnatal plasticity. Cell 134:508-520.
895 Swiech L, Heidenreich M, Banerjee A, Habib N, Li Y, Trombetta J, Sur M, Zhang F (2015) In
896 vivo interrogation of gene function in the mammalian brain using CRISPR-Cas9. Nat
897 Biotechnol 33:102-106.
898 Tan T, Wang W, Liu T, Zhong P, Conrow-Graham M, Tian X, Yan Z (2021) Neural circuits and
899 activity dynamics underlying sex-specific effects of chronic social isolation stress. Cell
900 Rep 34:108874.
901 Ueno H, Suemitsu S, Okamoto M, Matsumoto Y, Ishihara T (2017) Parvalbumin neurons and
902 perineuronal nets in the mouse prefrontal cortex. Neuroscience 343:115-127.
903 Ueno H, Takao K, Suemitsu S, Murakami S, Kitamura N, Wani K, Okamoto M, Aoki S, Ishihara
904 T (2018) Age-dependent and region-specific alteration of parvalbumin neurons and
905 perineuronal nets in the mouse cerebral cortex. Neurochem Int 112:59-70.
906 Wikenheiser AM, Schoenbaum G (2016) Over the river, through the woods: cognitive maps in
907 the hippocampus and orbitofrontal cortex. Nat Rev Neurosci 17:513-523.
908 Wohr M, Orduz D, Gregory P, Moreno H, Khan U, Vorckel KJ, Wolfer DP, Welzl H, Gall D,
909 Schiffmann SN, Schwaller B (2015) Lack of parvalbumin in mice leads to behavioral
910 deficits relevant to all human autism core symptoms and related neural morphofunctional
911 abnormalities. Transl Psychiatry 5:e525.
912 Won H, Lee HR, Gee HY, Mah W, Kim JI, Lee J, Ha S, Chung C, Jung ES, Cho YS, Park SG,
913 Lee JS, Lee K, Kim D, Bae YC, Kaang BK, Lee MG, Kim E (2012) Autistic-like social
914 behaviour in Shank2-mutant mice improved by restoring NMDA receptor function.
915 Nature 486:261-265.

916 Yizhar O, Fenno LE, Prigge M, Schneider F, Davidson TJ, O'Shea DJ, Sohal VS, Goshen I,
917 Finkelstein J, Paz JT, Stehfest K, Fudim R, Ramakrishnan C, Huguenard JR, Hegemann
918 P, Deisseroth K (2011) Neocortical excitation/inhibition balance in information
919 processing and social dysfunction. Nature 477:171-178.
920 Yoo T, Cho H, Park H, Lee J, Kim E (2019) Shank3 Exons 14-16 Deletion in Glutamatergic
921 Neurons Leads to Social and Repetitive Behavioral Deficits Associated With Increased
922 Cortical Layer 2/3 Neuronal Excitability. Front Cell Neurosci 13:458.
923

924 **Figure legends**

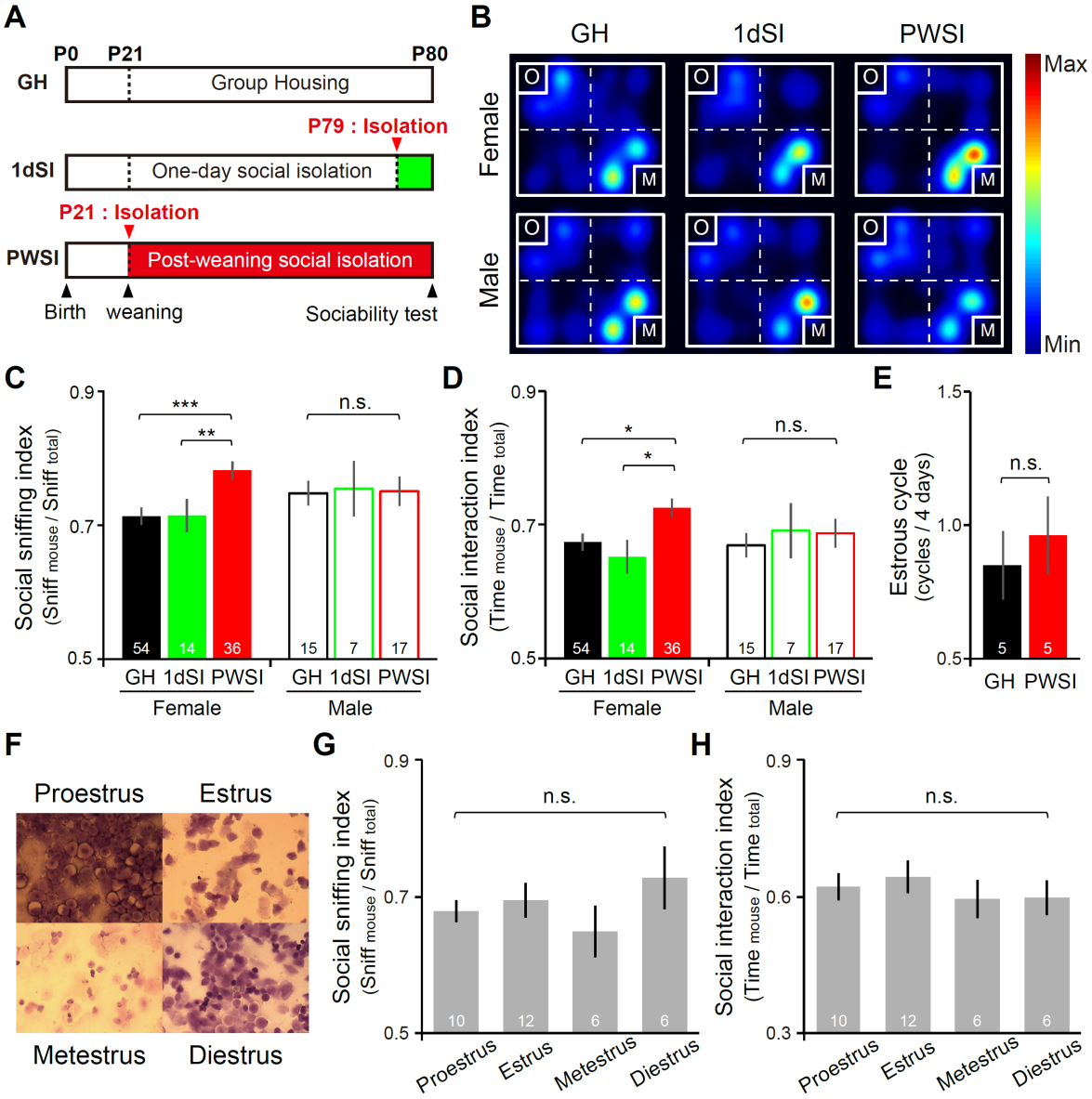

925

926 **Fig 1. PWSI during adolescence enhances social approaching behavior in female mice.**

927 (A) Experimental design of the sociability test. Schematic of group housing (GH), 1day social

928 isolation (1dSI), and post-weaning social isolation (PWSI). Note that the sociability behavior was

929 measured at P80.

930 (B) Representative heatmaps indicating mouse locations in the square chamber during the
931 sociability test. In the chamber, a container containing a novel object (O) and a container
932 containing the same-sex novel mouse (M) were located at diagonal corners. Heatmaps were
933 calculated in EthoVision XT as the mean duration of time spent in an area for each group.
934 (C) The social sniffing index displays the social sniffing times divided by the total sniffing times.
935 One-way ANOVA test, female, $F_{(2, 101)} = 8.431$, ***$p < 0.001$; male, $F_{(2, 36)} = 0.015$, $p = 0.985$,
936 Fisher's least significant difference post hoc test (female, GH vs PWSI, ***$p < 0.001$; 1dSI vs
937 PWSI, **$p = 0.009$; GH vs 1dSI, $p = 0.967$). Note that only the PWSI female mice showed a
938 significant increase in social sniffing behavior.
939 (D) The social interaction index displays the time spent in the social zone divided by the total time
940 spent in both object and social interaction zones. One-way ANOVA test, female, $F_{(2, 101)} = 3.496$,
941 *$p = 0.034$; male, $F_{(2, 36)} = 0.109$, $p = 0.897$, Fisher's least significant difference post hoc test
942 (female, GH vs PWSI, *$p = 0.027$; 1dSI vs PWSI, *$p = 0.031$; GH vs 1dSI, $p = 0.494$). Note that
943 only the PWSI female mice showed a significant increase in social interaction behavior.
944 (E) The number of estrous cycles per 4 days of GH ($n = 5$) and PWSI mice ($n = 5$). The duration
945 of estrous cycles was not different between groups. Mann-Whitney U test, $p = 0.912$.
946 (F) Representative images of cells in the vaginal smear that were stained with crystal violet. The
947 estrous cycles of female mice were identified based on the shape of stained cells.
948 (G) The social sniffing indices of females across the estrous cycle. One-way ANOVA test, $F_{(3,30)}$
949 $= 0.927$, $p = 0.440$.
950 (H) The social interaction indices of females across the estrous cycle. One-way ANOVA test, $F_{(3,30)}$
951 $= 0.513$, $p = 0.677$.

952 All data are presented as mean ± SEM. For (C-D), Female, GH, n = 54 mice, 1dSI, n = 14 mice,
953 PWSI, n = 36 mice; Male, GH, n = 15 mice, 1dSI, n = 7 mice, PWSI, n = 17 mice; For (G-H),
954 Proestrus, n = 10 mice, Estrus, n = 12 mice, Metestrus, n = 6 mice, Diestrus, n = 6 mice. *** $p < 0.001$, ** $p < 0.01$, * $p < 0.05$, n.s., not significant.
955
956

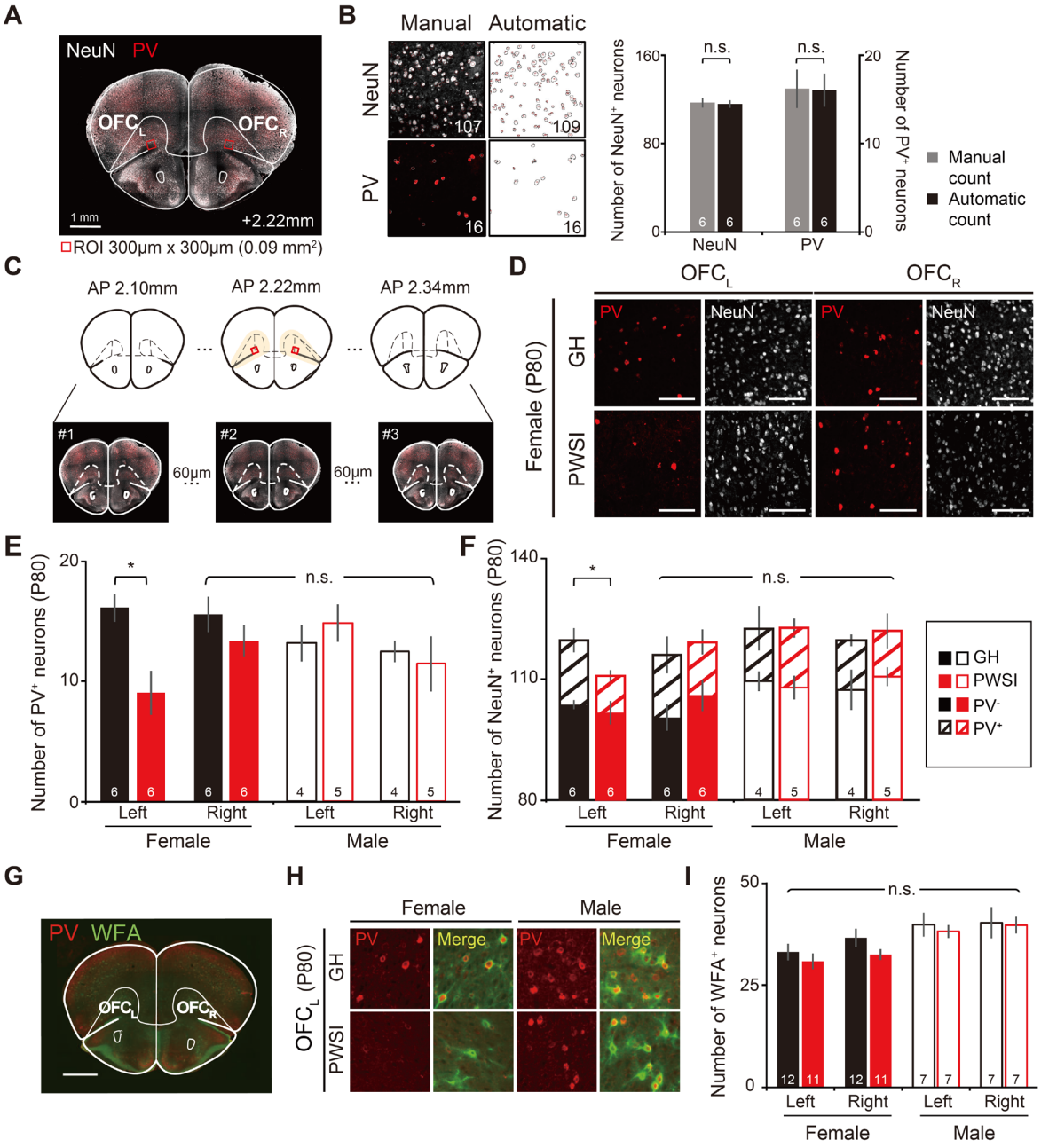

957

958 **Fig 2. PV expression in the OFC_L decreases in the PWSI female mice.**

959 (A) A representative image of the immunostained PV and NeuN in the OFC of a mouse brain

960 coronal section marked with the regions of interest (ROI, 0.09 mm^2). Scale bar, 1 mm.

961 (B) Validation of the automatic cell counting method. Left, representative images of the NeuN
962 (white) and PV (red) immunostained in the OFC_L of GH female mice. The left panels show original
963 images used for manual counting, and the right panels show automatically detected cell boundaries
964 from original images. The bottom numbers indicate the counted cell numbers. Right, the average
965 numbers of $NeuN^+$ and PV^+ neurons in the OFC_L of GH female mice from the manual counting
966 (gray) and automatic counting (black) (n = 6). Note that there is no difference between numbers
967 from manual and automatic counting. Mann-Whitney U test, NeuN, p = 0.200; PV, p = 1.000.
968 (C) Schematic brain images showing the selection of brain slices for cell counting. Three brain
969 slices were selected between AP +2.1mm and +2.34mm with an interval of 60μm.
970 (D) Representative fluorescence images of the PV (red) and the NeuN (white) immunostained in
971 the OFC_L and OFC_R of P80 GH and PWSI female mice. Scale bars, 100μm.
972 (E) The number of PV^+ neurons in the OFC. PWSI decreased the number of PV^+ neurons in the
973 female OFC_L. Mann-Whitney U test, female left, *p = 0.030; female right, p = 0.297; male left, p
974 = 0.623; male right, p = 1.000.
975 (F) The number of $NeuN^+$ neurons in the OFC. Mann-Whitney U test, female left, *p = 0.024,
976 female right, p = 1.000, male left, p = 0.903; male right, p =1.000. Slashed bars indicate the
977 number of PV^+ ($NeuN^+$) neurons and filled bars indicate PV^- ($NeuN^+$) neurons. Note that, PWSI
978 female mice showed a selective reduction in PV^+ ($NeuN^+$) neurons in OFC_L.
979 (G) A representative image of a mouse coronal brain section that was immunostained for PV (red)
980 and WFA (green) (scale bar, 1000μm).
981 (H) Representative fluorescence images of the OFC_L immunostained with anti-PV and anti-WFA
982 antibodies.

983 (I) The number of WFA^+ neurons in the OFC left and right of male and female mice. Mann-
984 Whitney U test, GH vs. PWSI, female left, $p = 0.46$; female right, $p = 0.185$; male left, $p = 0.337$;
985 male right, $p = 0.442$.
986 All data are presented as mean ± SEM. GH, group-housed mice; PWSI, mice isolated from P21 to
987 P80. For (E-F), Female, GH, $n = 6$ mice, PWSI, $n = 6$ mice; Male, GH, $n = 4$ mice, PWSI, $n = 5$
988 mice. For (H-J), Female, GH, $n = 12$ mice, PWSI, $n = 11$ mice; Male, GH, $n = 7$ mice, PWSI, n
989 $= 7$ mice. *$p < 0.05$, n.s., not significant.
990

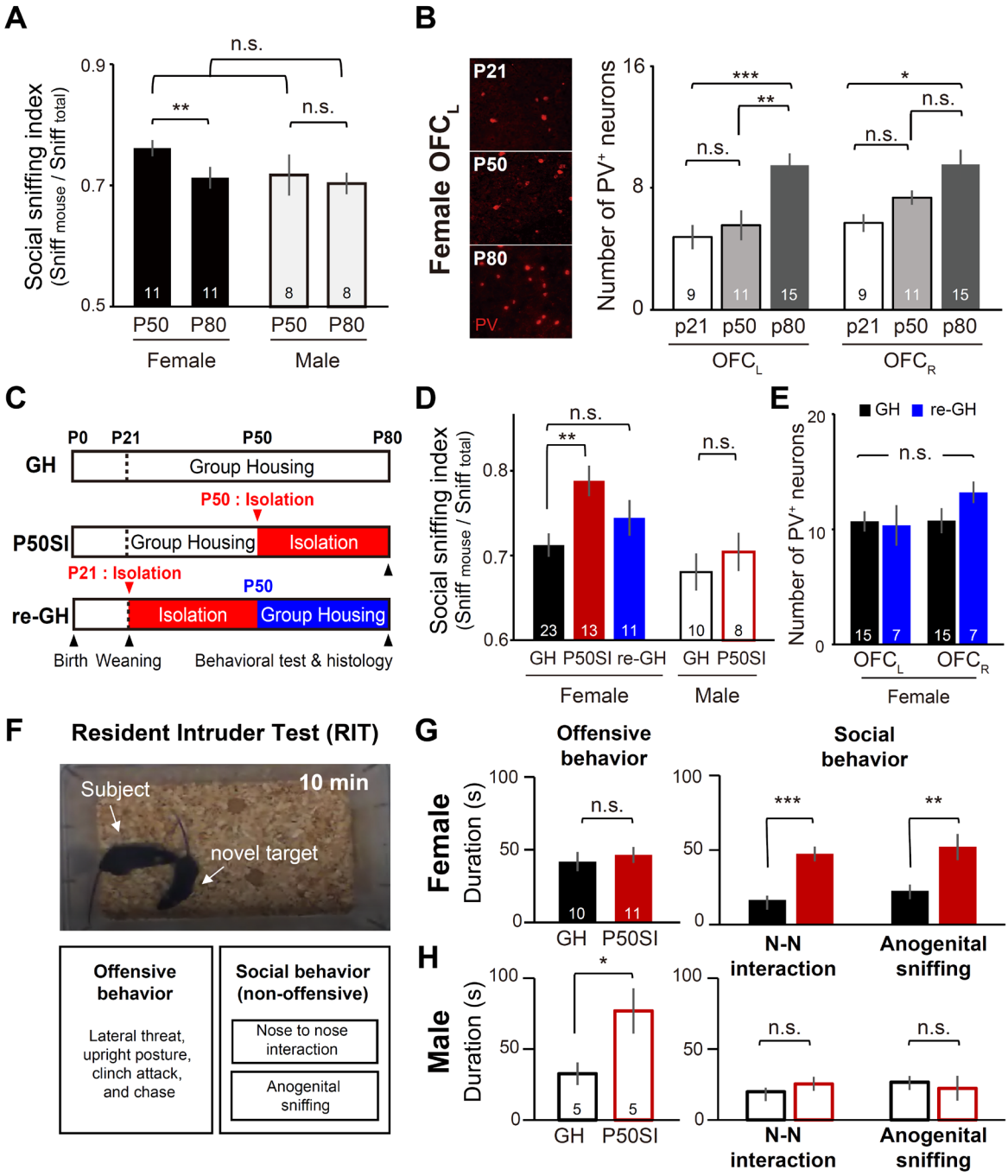

991

992 **Fig 3. Social isolation during late adolescence causes hypersociability only in female mice**

993 (A) The social sniffing indices of GH female and male mice. The sociability test was performed

994 at P50 and P80 in the same mouse. Paired, Student's t-test within a group, female, **p = 0.008;

995 male, p = 0.756. Unpaired, Student's t-test between groups, P50, p = 0.285; P80, p = 0.731. Female,
996 *n* =11 mice; Male, *n* =8 mice.
997 (B) Left, representative fluorescence images of the OFC_L immunostained with anti-PV antibodies
998 (red). Brain sections were collected from P21 (top), P50 (middle), and P80 (bottom) GH female
999 mice. Right, the number of PV^+ neurons in the OFC_L and OFC_R of female mice. One-way ANOVA
1000 test, female OFC_L, $F_{(2, 32)} = 8.473$, **p=0.001, Fisher's least significant difference post hoc test
1001 (P21 vs P50, p = 0.580; P50 vs P80, **p = 0.003; P21 vs P80, ***p < 0.001); female OFC_R, $F_{(2, 28)}$
1002 = 2.856, *p = 0.010, Fisher's least significant difference post hoc test (P21 vs P50, p = 0.204; P50
1003 vs P80, p = 0.065; P21 vs P80, **p = 0.003). Female, P21, *n* = 9 mice; P50, *n* = 11 mice; P80, *n* =
1004 15 mice.
1005 (C) Schematic of group-housing (GH), social isolation from P50 to P80 (P50SI), and re-group-
1006 housing at P50 after social isolation at P21 (re-GH). Note that the behavioral tests were performed
1007 at P80.
1008 (D) The social sniffing indices of GH, P50SI, and re-GH mice. One-way ANOVA test, female, $F_{(2,}$
1009 $_{44)} = 5.069$, *p = 0.01, Fisher's least significant difference post hoc test (female, GH vs P50SI, **p
1010 = 0.007; GH vs re-GH, p = 0.276; P50SI vs re-GH, p = 0.127). Mann-Whitney U test, male, GH
1011 vs P50SI, p = 0.505. Note that only the P50SI female mice showed a significant increase in social
1012 sniffing behavior compared to GH female mice. Female, GH, *n* = 23 mice, P50SI, *n* = 13 mice,
1013 re-GH, *n* = 11 mice; Male, GH, *n* = 10 mice, P50SI, *n* = 8 mice.
1014 (E) The number of PV^+ neurons in the OFC of GH (black) and re-GH (blue) female mice. Unpaired,
1015 Student's t-test, OFC left, p = 0.873; OFC right, p = 0.120. Female, GH, *n* = 15 mice; re-GH, *n* =
1016 7 mice.

1017 (F) The resident-intruder test (RIT) was performed for P50SI and GH female and male mice at
1018 P80. Top, a representative image of RIT. Bottom, the list of analyzed behaviors. The offensive
1019 behavior included lateral threat, upright posture, clinch attack, and chase. The social behavior
1020 included nose to nose interaction (N-N interaction) and anogenital sniffing.
1021 (G) The RIT results of GH and P50SI female mice. Left, duration of offensive behaviors. Mann-
1022 Whitney U test, $p = 0.699$. Right, duration of social behaviors. Mann-Whitney U test, N-N
1023 interaction, ***$p < 0.001$; anogenital sniffing, **$p = 0.008$. Female P50SI mice showed a
1024 significant increase in social behaviors without any change in offensive behaviors.
1025 (H) The RIT results of GH and P50SI male mice. Left, duration of offensive behaviors. Mann-
1026 Whitney U test, *$p = 0.037$. Right, duration of social behaviors. Mann-Whitney U test, N-N
1027 interaction, $p = 0.095$; anogenital sniffing, $p = 0.835$. Male P50SI mice showed a significant
1028 increase in offensive behaviors without any change in social behaviors.
1029 All data are presented as mean ± SEM. For (F-H), Female, GH, $n = 11$ mice, P50SI, $n = 11$ mice;
1030 Male, GH, $n = 5$ mice, P50SI, $n = 5$ mice. ***$p < 0.001$, **$p < 0.01$, *$p < 0.05$, n.s., not significant.
1031

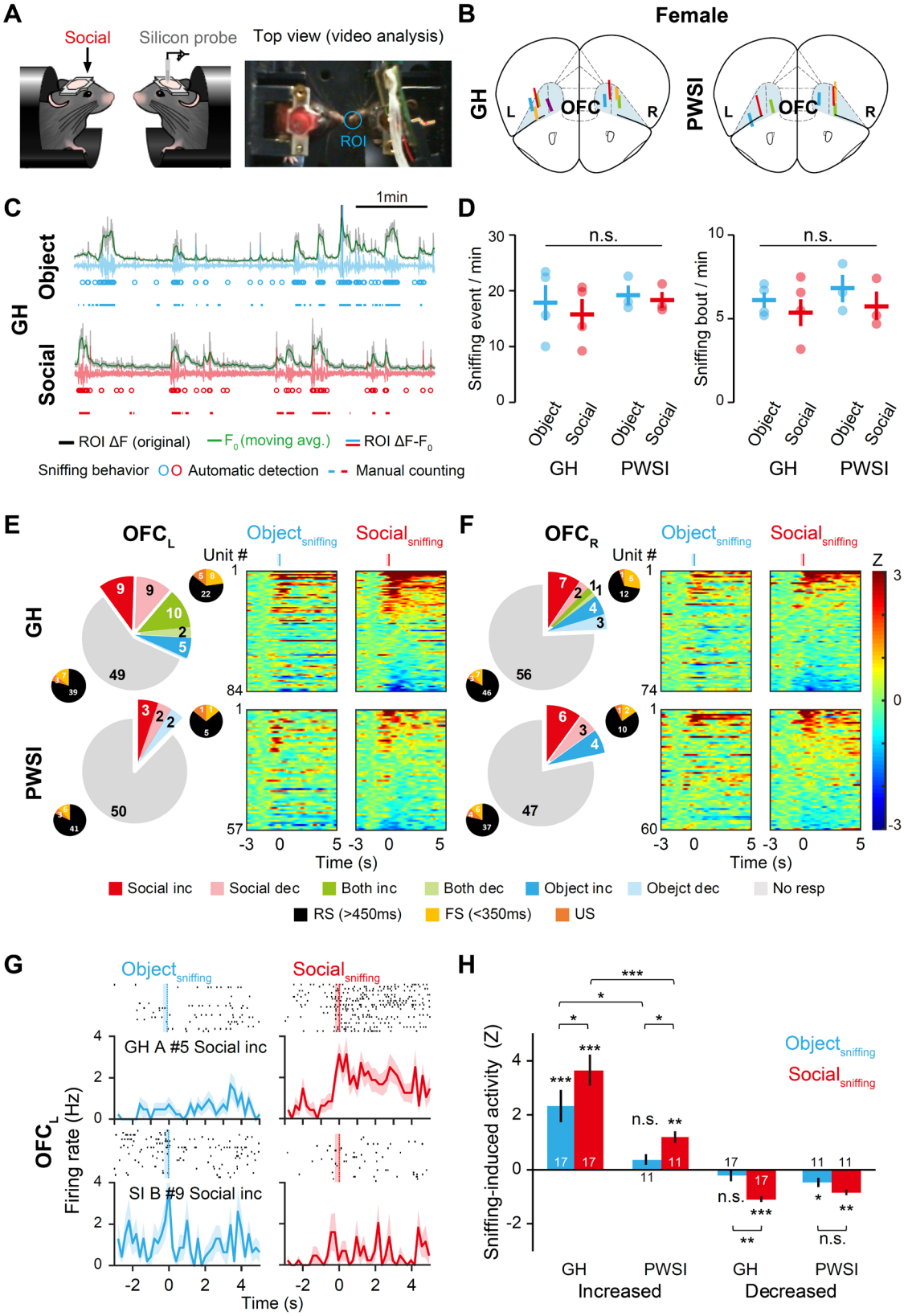
A
Social
Silicon probe
Top view (video analysis)
ROI
B
Female
GH
PWSI
L
OFC
R
C
1min
Object
Social
GH
ROI ΔF (original)
F0 (moving avg.)
ROI ΔF-F0
Sniffing behavior
Automatic detection
Manual counting
D
n.s.
Sniffing event / min
Sniffing bout / min
Object
Social
GH
PWSI
E
OFCL
Objectsniffing
Socialsniffing
Unit #
Time (s)
F
OFCR
Z
Social inc
Social dec
Both inc
Both dec
Object inc
Obejct dec
No resp
RS (>450ms)
FS (<350ms)
US
G
GH A #5 Social inc
SI B #9 Social inc
Firing rate (Hz)
H
Sniffing-induced activity (Z)
Increased
Decreased
n.s.

1032

1033 **Fig 4. PWSI reduces sniffing-induced activity in the OFC_L of female mice.**

1034 (A) Left, experimental design for *in vivo* multichannel recording of the neurons responsive to
1035 social sniffing in the OFC of head-fixed mice. Right, a representative top view image for video
1036 analysis. The blue circle indicates the region of interest (ROI) used to analyze the brightness
1037 changes in the video clip.

1038 (B) Schematic illustration of mouse brain sections marked with the recording sites in the OFC of
1039 GH or PWSI female mice. Blue shading, OFC; colored bars, recording sites confirmed by post hoc
1040 histology.

1041 (C) Representative sniffing events measured in GH female mice. Gray trace, raw brightness
1042 changes in the ROI (ROI ΔF). Green trace, moving average in the ROI (F_0, sliding window = 50
1043 frames). Blue and red trace, normalized brightness changes in the ROI (ROI $\Delta F–F_0$). Circles,
1044 sniffing events were automatically detected by a Matlab-based image analysis code. Horizontal
1045 lines, sniffing events manually detected by an observer in the EthoVision XT software. Note that
1046 automatic counting methods detect sniffing events at similar times identified by manual counting.
1047 Blue, object sniffing; red, social sniffing.

1048 (D) Left, sniffing events automatically counted. Dots, individual data; lines, means ± SEM.
1049 Wilcoxon signed-rank test within a group, Object vs. Social, GH, $p = 0.465$, PWSI, $p = 1.000$.
1050 Mann-Whitney U test between groups, GH vs. PWSI, Object, $p = 0.857$, Social, $p = 0.629$. Right,
1051 the sniffing events manually identified. Dots, individual data; lines, means ± SEM. Wilcoxon
1052 signed-rank test within a group, Object vs. Social, GH, $p = 0.686$, PWSI, $p = 0.109$. Mann-
1053 Whitney *U* test between groups, GH vs. PWSI, Object, $p = 0.393$, Social, $p = 1.000$. GH, $n = 4$
1054 mice, PWSI, $n = 3$ mice.

1055 (E) Neural responses associated with sniffing in the female OFC_L. The large pie charts, the OFC_L
1056 neurons showing social sniffing responses (Social, red), object sniffing responses (Object, blue),
1057 or both social and object sniffing responses (Both, green). Inc and dec, neurons showing
1058 significantly increased and decreased activities after the onset of sniffing, respectively ($p < 0.01$,
1059 bootstrap); No resp., neurons that show no responses. The small pie charts, the waveforms of the
1060 responsive (right-top) and non-responsive (left-bottom) OFC_L neurons classified according to the
1061 waveform width. RS, regular-spiking neurons with a waveform width >450ms; FS, fast-spiking
1062 neurons with a waveform width <350ms; US, unclassified neurons with a waveform width
1063 between 350ms and 450ms. Heatmaps, *Z*-scored activity of all neurons normalized by the pre-
1064 sniffing activity. GH, $n = 5$ mice, $n = 84$ units; PWSI, $n = 3$ mice, $n = 57$ units.
1065 (F) The same as (C) but for the OFC_R neurons. GH, $n = 4$ mice, $n = 74$ units; PWSI, $n = 4$ mice,
1066 $n = 60$ units.
1067 (G) Representative raster plots and peri-event time histograms of example 'Social Inc' OFC_L
1068 neurons from the GH female mouse (top, GH A #5) and from the PWSI female mouse (bottom, SI
1069 B #9) aligned by the onset of object sniffing (left, blue) and the onset of social sniffing (right, red).
1070 (H) Averaged sniffing-induced activity for 2 sec (*Z* score) of the top 20% of OFC_L neurons that
1071 show either increased or decreased responses after the onset of social sniffing. Bars, means ± SEM.
1072 Wilcoxon signed-rank test for each bar, $Object_{sniffing}$, $Social_{sniffing}$, ***$p < 0.001$, ***$p < 0.001$ for
1073 GH Increased; $p = 0.083$, **$p = 0.004$ for PWSI Increased; $p = 0.478$, ***$p < 0.001$ for GH
1074 Decreased; *$p = 0.045$, **$p = 0.004$ for PWSI Decreased. Wilcoxon signed-rank test within a
1075 group ,$Object_{sniffing}$ vs. $Social_{sniffing}$, *$p = 0.047$ for GH Increased; *$p = 0.023$, for PWSI Increased;
1076 **$p = 0.002$ for GH Decreased; $p = 0.120$ for PWSI Decreased; Mann-Whitney U test between
1077 groups ,$Object_{sniffing}$, $Social_{sniffing}$, *$p = 0.019$, ***$p < 0.001$ for Increased activity; $p = 0.452$, p =

1078 0.110 for Decreased activity. GH, n = 17 units, PWSI, n = 11 units. ***$p < 0.001$, **$p < 0.01$, *p

1079 < 0.05, n.s., not significant.

1080

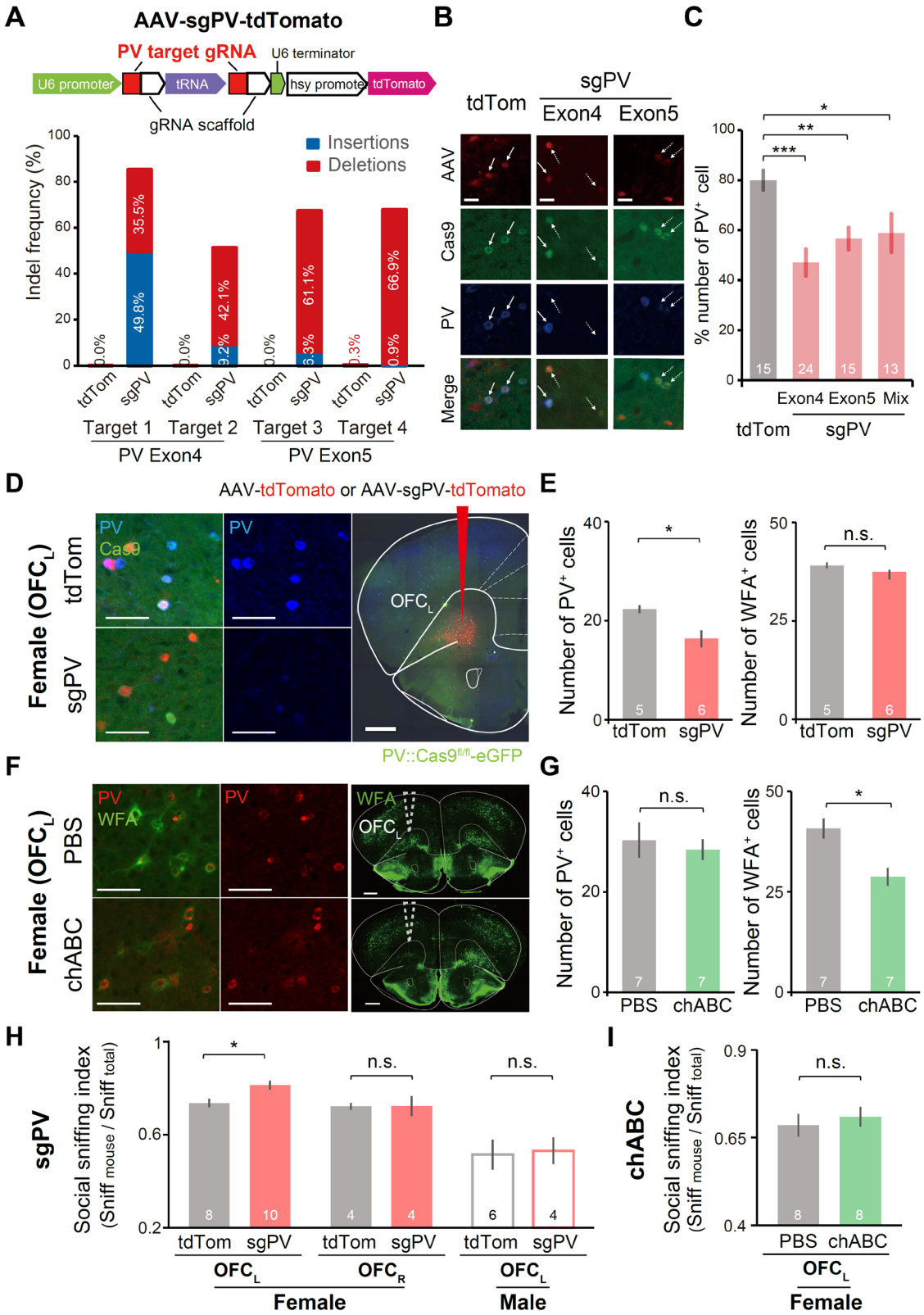

Fig 5. CRISPR/Cas9-mediated knock-down of PV, but not PNN degradation, in the OFCL

1083 **enhances sociability in female mice.**

1084 (A) Top, schematic illustration of the AAV-sgPV-tdTomato expression vector. The sgRNA vector
1085 contains the encoding sequence of tdTomato protein for identifying transduced neurons. We used
1086 two types of AAVs to target both exon 4 and exon5 of the PV gene. Bottom, DNA insertion (blue)
1087 and deletion (red) mutation ratio (Indel frequency) by the designed sgPVs targeting exon 4 and
1088 exon5 of the PV gene and cloned in the AAV-tdTom vector.

1089 (B) Representative PV-immunostained images of PV::Cas9 mice injected with AAV-tdTomato or
1090 AAV-sgPV-tdTomato. Scale bars, 20μm. Red, tdTomato expressed by AAV vectors; green, Cas9-
1091 eGFP transgenically expressed in PV^+ neurons; blue, immunostained PV proteins. Solid arrows
1092 indicate triple-positive cells, and dashed arrows indicate double-positive and PV-negative cells.

1093 (C) Quantification of PV^+ cells among eGFP and tdTomato double-positive cells in the
1094 retrosplenial cortex (RSC), injected with AAVs that deliver tdTom or sgPVs, compared to the
1095 Cas9-eGFP expression in PV::Cas9 mice. Numbers in columns indicate the number of brain
1096 samples analyzed. One-way ANOVA, $F_{(3, 63)} = 6.478$, ***$p < 0.001$; Fisher's least significant
1097 difference post hoc test.

1098 (D) CRISPR/Cas9-mediated knock-down of PV in the female OFC_L. Left and middle,
1099 representative fluorescence images of the OFC_L of the female PV::Cas9-eGFP mice injected with
1100 the AAV-tdTomato (top, tdTom) or AAV-sgPV-tdTomato (bottom, sgPV). Red, tdTomato; green,
1101 Cas9-eGFP; blue, immuno-stained PV. Scale bars, 50μm. Right, a representative image of the
1102 OFC_L of a PV::Cas9-eGFP mouse injected with the AAV-sgPV-tdTomato. Scale bar, 1000μm.

1103 (E) The number of PV^+ and WFA^+ neurons in the OFC_L injected with the AAV-tdTomato (gray
1104 bars) or with the AAV-sgPV-tdTomato (red bars). Mann-Whitney U test, PV, *$p = 0.022$; WFA,
1105 $p = 0.306$. Female, $n = 5$ mice for tdTom, $n = 6$ mice for sgPV.

1106 (F) chABC-induced PNN degradation in the OFC_L of female mice. Left and middle,
1107 immunostained PV (red) and WFA (green) in the OFC_L of female mice injected with PBS (top) or
1108 chABC (bottom). Scale bars, 50μm. Right, representative fluorescence images of the PNN stained
1109 with the WFA Note that the chABC injection selectively degraded PNNs in the OFC_L. Scale bars,
1110 1000μm.
1111 (G) The number of PV^+ and WFA^+ neurons in the OFC_L injected with the PBS (gray bars) or the
1112 chABC (green bars). Mann-Whitney U test, PV, p = 0.609; WFA, *p = 0.017. Female, *n* = 7 mice
1113 for PBS, *n* = 7 mice for chABC
1114 (H) Social sniffing indices of PV::Cas9 female mice injected with AAV-tdTomato (tdTom) or
1115 AAV-sgPV-tdTomato (sgPV). Mann-Whitney U test, tdTom vs sgPV, female OFC_L, *p = 0.021;
1116 female OFC_R, p = 0.885; male OFC_L, p = 0.914. tdTom, female OFC_L, *n* = 8 mice; female OFC_R,
1117 *n* = 4 mice, male OFC_L, *n* = 6 mice; sgPV, red, female OFC_L, *n* = 10 mice; female OFC_R, *n* = 4
1118 mice, male OFC_L, *n* = 4 mice.
1119 (I) Social sniffing indices of mice injected with PBS (gray) or chABC (green). Mann-Whitney U
1120 test, p = 0.878. PBS, *n* = 8 mice; chABC, *n* = 8.
1121 All data are presented as mean ± SEM. *p < 0.05, n.s., not significant.
1122

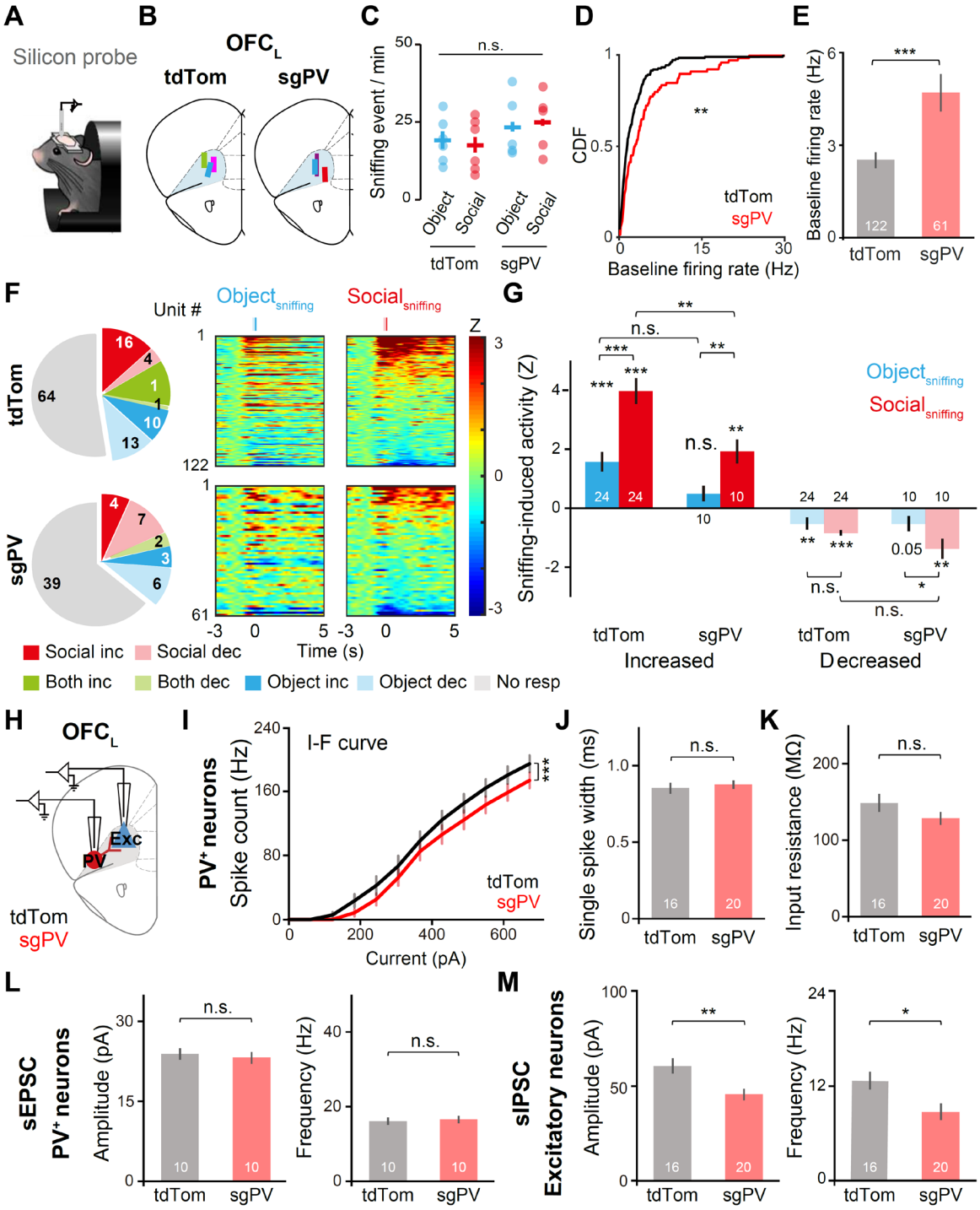

Fig 6. Knock-down of PV reduces sniffing-induced activity and decreases synaptic inhibition in the female OFC$_L$.

1126 (A) Schematic illustration of *in vivo* multichannel recording in a head-fixed mouse.

1127 (B) Schematic illustration of coronal brain sections of *in vivo* recording sites in the OFC_L where

1128 tdTomato (tdTom)- or PV sgRNA (sgPV)-expressing AAVs were injected.

1129 (C) Sniffing events automatically counted for tdTom and sgPV mice. Left, Wilcoxon signed-rank

1130 test for within a group, tdTom, $p = 0.463$; sgPV, $p = 0.892$. Mann-Whitney U test between groups,

1131 Object, $p = 0.537$; Social, $p = 0.126$.

1132 (D) The cumulative distribution function of baseline firing rates in tdTom and sgPV mice. Baseline

1133 firing rates were calculated as the mean firing rates for 2 sec before the sniff onset. Kolmogorov–

1134 Smirnov test, $^{**}p = 0.006$.

1135 (E) Mean baseline firing rates of tdTom and sgPV mice. Mann-Whitney U test, $^{***}p < 0.001$.

1136 (F) Neural responses associated with the sniffing in the OFC_L of tdTom- (top) or sgPV-(bottom)

1137 injected PV::Cas9 female mice. Pie charts, the OFC_L neurons showing social sniffing responses

1138 (Social, red), object sniffing responses (Object, blue), or both social and object sniffing responses

1139 (Both, green). Inc and dec, neurons showing significantly increased and decreased activities after

1140 the onset of sniffing, respectively ($p < 0.01$, bootstrap); No resp, neurons that show no responses.

1141 Heatmaps, Z-scored activity of all recorded neurons by the pre-sniffing activity. Note that the

1142 number of sniffing-responsive neurons and social sniffing-induced activity was reduced in sgPV

1143 females. Heat maps, *Z*-scored activity of all neurons normalized by the pre-sniffing activity.

1144 (G) Averaged sniffing-induced activity for 2 sec (*Z* score) of the top 20% of OFC_L neurons that

1145 show either increased or decreased responses after the onset of social sniffing. Wilcoxon signed-

1146 rank test for each bar, $Object_{sniffing}$, $Social_{sniffing}$, $^{***}p < 0.001$, $^{***}p < 0.001$ for tdTom Increased;

1147 $p = 0.154$, $^{**}p = 0.006$ for sgPV Increased; $^{**}p = 0.007$, $^{***}p < 0.001$ for tdTom Decreased; p

1148 $= 0.053$, $^{**}p = 0.006$ for sgPV Decreased. Note that the increased neurons showed larger activity

1149 changes after social sniffing than after object sniffing. Wilcoxon signed-rank test within a group,
1150 $Object_{sniffing}$ vs $Social_{sniffing}$, ***$p < 0.001$ for tdTom Increased; **$p = 0.008$ for sgPV Increased;
1151 $p = 0.141$ for tdTom Decreased; *$p = 0.011$ for sgPV Decreased. The social sniffing-induced
1152 activity was larger in tdTom females than in sgPV females. Mann-Whitney U test between groups,
1153 $Object_{sniffing}$, $Social_{sniffing}$, $p = 0.067$, **$p = 0.004$ for Increased activity; $p = 0.720$, $p = 0.073$ for
1154 Decreased activity. tdTom, $n = 24$ units, sgPV, $n = 12$ units.
1155 (H) Physiological properties of PV^+ neurons expressed with tdTom or sgPV. Schematic illustration
1156 of the whole-cell patch-clamp recordings of PV^+ neurons (red) or excitatory neurons (blue) in the
1157 PV::Cas9 mice injected with the AAVs expressing either tdTom or sgPV-tdTom into the OFC_L.
1158 (I) SgPV expression decreased the excitability of PV^+ neurons. Current-firing (I-F) curves
1159 measured in the OFC_L PV^+ neurons. sgPV expression caused a significant decrease in current-
1160 evoked spike counts in the PV^+ neurons. Two-way ANOVA, $F_{AAV\ (1,\ 372)} = 14.528$, ***$p < 0.001$,
1161 $F_{current\ (11,\ 372)} = 121.158$, ***$p < 0.001$, $F_{AAV\ x\ current\ (11,\ 372)} = 0.388$, $p = 0.960$.
1162 (J) Mean half-width of spikes (ms) measured in PV^+ neurons expressed with the tdTom or the
1163 sgPV. Unpaired, Student's t-test, $p = 0.628$.
1164 (K) Mean input resistance (MΩ) measured in PV^+ neurons expressed with the tdTom or the sgPV.
1165 Unpaired, Student's t-test, $p = 0.173$.
1166 (L) Spontaneous EPSCs measured in PV^+ neurons of the OFC_L. Left bars, mean amplitudes (pA)
1167 of sEPSCs in PV^+ neurons. Unpaired, Student's t-test, $p = 0.636$. Right bars, mean frequency (Hz)
1168 of sEPSCs in PV^+ neurons. Unpaired, Student's t-test, $p = 0.940$. tdTom = 10 cells (5 mice);
1169 sgPV=10 cells (4 mice); female.
1170 (M) Spontaneous IPSCs measured in excitatory neurons of the OFC_L. Left bars, mean amplitudes
1171 (pA) of sIPSCs in Pyr neurons. Unpaired, Student's t test, **$p = 0.006$. Right bars, mean

1172 frequencies (Hz) of sIPSCs in Pyr neurons. Unpaired, Student's t test, *p = 0.015. tdTom = 16

1173 cells (3 mice); sgPV=17 cells (3 mice); female.

1174 All data are presented as mean ± SEM. For (D-G), tdTom: *n* = 6 mice, *n* = 122 units, sgPV: *n* = 5

1175 mice, *n* = 61 units. For (I-K), tdTom = 16 cells (3 mice); sgPV = 20 cells (4 mice); female. ***p

1176 < 0.001, **p < 0.01, *p < 0.05, n.s., not significant.

1177

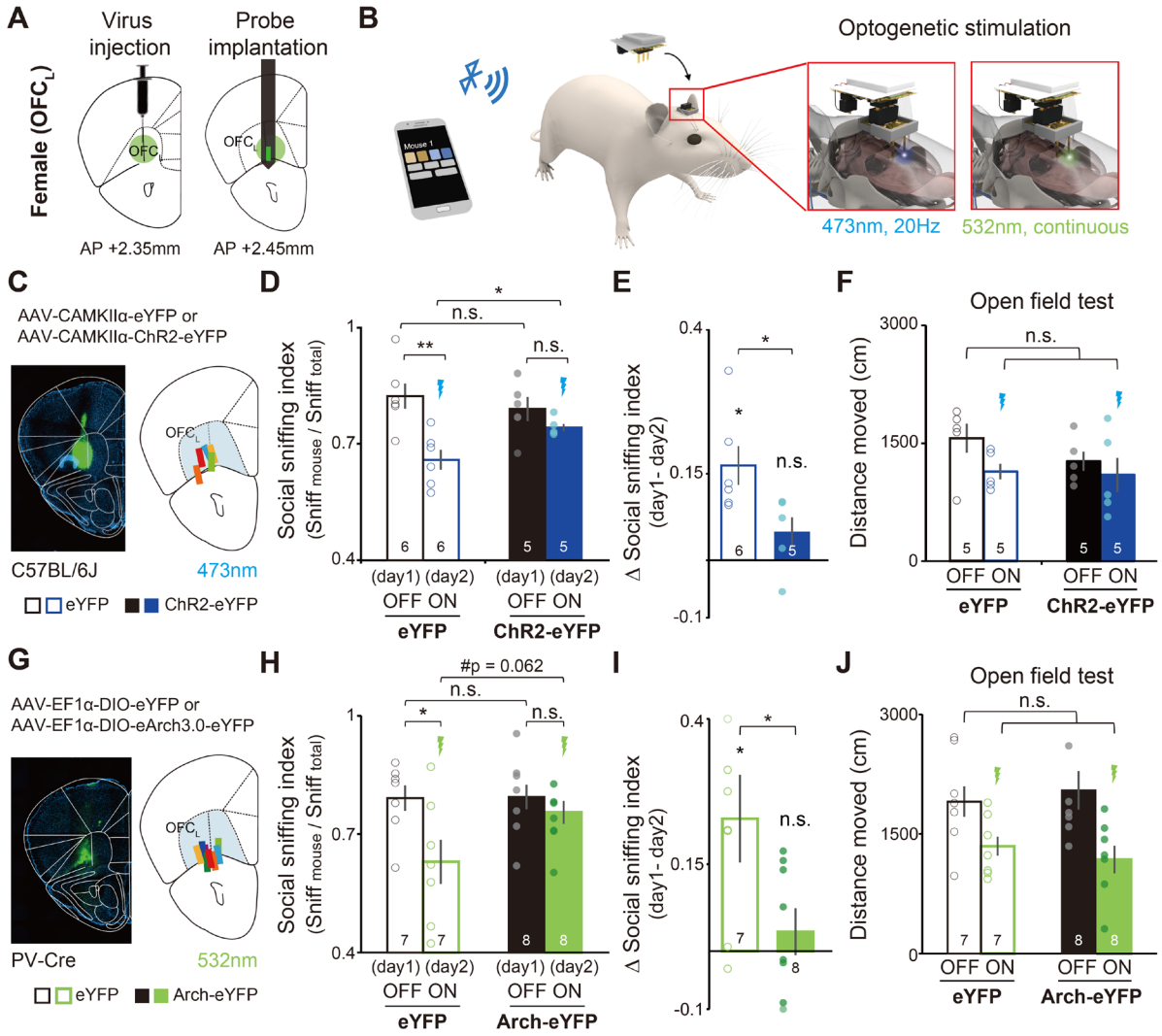

Fig 7. Optogenetic activation of excitatory neurons or inhibition of PV$^+$ neurons in the OFC$_L$ caused hypersociability in female mice.

(A) Schematic illustration of virus injection and probe implantation for wireless optogenetic manipulation. The virus was injected into the OFC$_L$ of a mouse. After a week of recovery, the wireless LED probe was implanted in the anterior part of OFC$_L$ of a mouse.

(B) Schematic illustration of wireless optogenetic manipulation. The smartphone application was used to turn on or off the light by Bluetooth Low Energy (BLE). For optogenetic stimulation, two

1186 types of LED light were used at different temporal modes: blue LED (473 nm) at a 20Hz light-
1187 pulse mode and green LED light (532nm) at a continuous light-on mode.
1188 (C) Optogenetic activation of excitatory neurons in the female OFC_L. AAV-CAMKIIα-
1189 eYFP(eYFP, open bars) or AAV-CAMKIIα-ChR2-eYFP (ChR2-eYFP, filled bars) was injected
1190 into the OFC_L of PV-Cre female mice. Left, a representative brain image of the OFC_L of a WT
1191 female mouse injected with the AAV-CAMKIIα-ChR2-eYFP. Green, ChR2-eYFP; blue, DAPI.
1192 Right, a schematic illustration of a mouse brain section marked with each probe-implanted site in
1193 the OFC of ChR2-eYFP injected female mice. Blue shading, OFC; colored bars, probe-implanted
1194 sites confirmed by *post hoc* histology.
1195 (D) The social sniffing index of eYFP (open bars) and ChR-2eYFP (filled bars) mice was measured
1196 on two consecutive days. For Day1, the light was not delivered (OFF), and the social sniffing index
1197 was not different between the eYFP and ChR2-eYFP groups. Unpaired, Student's t-test between
1198 groups, $p = 0.516$. For Day2, the light was delivered to the OFC_L (ON), and ChR2-eYFP group
1199 showed a higher social sniffing index than eYFP group. Unpaired, Student's t-test between groups,
1200 $*p = 0.030$; Paired, Student's t-test within a group, eYFP, $**p = 0.007$; ChR2-eYFP, $p = 0.179$.
1201 (E) ΔSocial sniffing index indicates the difference in social sniffing index between day 1 (OFF)
1202 and day 2 (ON). Unpaired, Student's t-test between groups, $*p = 0.036$; Wilcoxon signed rank test
1203 for each group, eYFP, $*p = 0.036$; ChR2-eYFP, $p = 0.179$.
1204 (F) Locomotion of mice (distance moved (cm) for 5 min) in the open field chamber was not
1205 affected by the optogenetic activation of the OFC_L. Unpaired, Student's t-test between groups,
1206 OFF, $p = 0.267$; ON, $p = 0.874$. Paired, Student's t-test within a group, OFF vs ON, eYFP, $p =$
1207 0.078; ChR2-eYFP, $p = 0.602$. Female, eYFP; $n = 5$ mice; ChR2, $n = 5$ mice.

1208 (G) Optogenetic inactivation of PV^+ neurons in the female OFC_L. AAV-EF1α-DIO-eYFP (eYFP)
1209 or AAV-EF1α-DIO-eArch3.0-eYFP (Arch-eYFP) was injected into the OFC_L of PV-Cre female
1210 mice. Left, a representative brain image of the OFC_L of a PV-Cre female mouse injected with the
1211 AAV-EF1α-DIO-eArch3.0-eYFP. Green, Arch-eYFP; blue, DAPI. Right, a schematic illustration
1212 of a mouse brain section marked with each probe-implanted site in the OFC of Arch-eYFP injected
1213 female mice. Blue shading, OFC; colored bars, probe-implanted sites confirmed by *post hoc*
1214 histology.
1215 (H) The social sniffing index of eYFP (open bars) and Arch-eYFP (filled bars) mice. For day 1,
1216 the light was not delivered (OFF), and the social sniffing index was not different between eYFP
1217 and Arch-eYFP groups. Unpaired, Student's t-test between groups, day 1, $p = 0.950$; day 2, #$p =$
1218 0.062. Paired, Student's t-test within a group, eYFP, *$p = 0.048$; ChR2-eYFP, $p = 0.480$.
1219 (I) ΔSocial sniffing index of eYFP and Arch-eYFP. Unpaired, Student's t-test between groups, *p
1220 $= 0.046$. Wilcoxon signed rank test for each group, eYFP, *$p = 0.047$; Arch-eYFP, $p = 0.547$.
1221 (J) Locomotion of mice (distance moved (cm) for 5 min) in the open field chamber was not affected
1222 by the optogenetic inactivation of the PV^+ neurons in OFC_L. Unpaired, Student's t-test between
1223 groups, $p = 0.068$. Paired, Student's t-test within a group, OFF vs ON, eYFP, **$p = 0.007$, Arch-
1224 eYFP, **$p = 0.003$.
1225 All data are presented as mean ± SEM. Dots indicate the individual data. The blue lightning sign
1226 indicates the delivery of light stimulation (20Hz, 473nm), and the green lightning sign indicates
1227 the delivery of light stimulation (continuous, 532nm). For (C-E), eYFP, $n = 6$; ChR2-eYFP, $n =$
1228 5; female mice. For (G-J), eYFP, $n = 7$; Arch-eYFP, $n = 8$; female mice. **$p < 0.01$, *$p < 0.05$,
1229 #$p < 0.1$, n.s., not significant.